remote sensing

MDPI

Review

Measurement of Total Dissolved Solids and Total Suspended Solids in Water Systems: A Review of the Issues, Conventional, and Remote Sensing Techniques

Godson Ebenezer Adjovu, Haroon Stephen, David James and Sajjad Ahmad *

Department of Civil and Environmental Engineering and Construction, University of Nevada, Las Vegas, NV 89154, USA; adjovg1@unlv.nevada.edu (G.E.A.); haroon.stephen@unlv.edu (H.S.); dave.james@unlv.edu (D.J.)
* Correspondence: sajjad.ahmad@unlv.edu; Tel.: +1-702-895-5456

Abstract: This study provides a comprehensive review of the efforts utilized in the measurement of water quality parameters (WQPs) with a focus on total dissolved solids (TDS) and total suspended solids (TSS). The current method used in the measurement of TDS and TSS includes conventional field and gravimetric approaches. These methods are limited due to the associated cost and labor, and limited spatial coverages. Remote Sensing (RS) applications have, however, been used over the past few decades as an alternative to overcome these limitations. Although they also present underlying atmospheric interferences in images, radiometric and spectral resolution issues. Studies of these WQPs with RS, therefore, require the knowledge and utilization of the best mechanisms. The use of RS for retrieval of TDS, TSS, and their forms has been explored in many studies using images from airborne sensors onboard unmanned aerial vehicles (UAVs) and satellite sensors such as those onboard the Landsat, Sentinel-2, Aqua, and Terra platforms. The images and their spectral properties serve as inputs for deep learning analysis and statistical, and machine learning models. Methods used to retrieve these WQP measurements are dependent on the optical properties of the inland water bodies. While TSS is an optically active parameter, TDS is optically inactive with a low signal–noise ratio. The detection of TDS in the visible, near-infrared, and infrared bands is due to some process that (usually) co-occurs with changes in the TDS that is affecting a WQP that is optically active. This study revealed significant improvements in incorporating RS and conventional approaches in estimating WQPs. The findings reveal that improved spatiotemporal resolution has the potential to effectively detect changes in the WQPs. For effective monitoring of TDS and TSS using RS, we recommend employing atmospheric correction mechanisms to reduce image atmospheric interference, exploration of the fusion of optical and microwave bands, high-resolution hyperspectral images, utilization of ML and deep learning models, calibration and validation using observed data measured from conventional methods. Further studies could focus on the development of new technology and sensors using UAVs and satellite images to produce real-time in situ monitoring of TDS and TSS. The findings presented in this review aid in consolidating understanding and advancement of TDS and TSS measurements in a single repository thereby offering stakeholders, researchers, decision-makers, and regulatory bodies a go-to information resource to enhance their monitoring efforts and mitigation of water quality impairments.

Keywords: airborne sensors; hyperspectral; multispectral; optically active; remote sensing (RS); satellite sensors; total dissolved solids (TDS); total suspended solids (TSS)

check for updates

Citation: Adjovu, G.E.; Stephen, H.; James, D.; Ahmad, S. Measurement of Total Dissolved Solids and Total Suspended Solids in Water Systems: A Review of the Issues, Conventional, and Remote Sensing Techniques. *Remote Sens.* **2023**, *15*, 3534. https://doi.org/10.3390/rs15143534

Academic Editor: Teodosio Lacava

Received: 25 May 2023
Revised: 11 July 2023
Accepted: 11 July 2023
Published: 13 July 2023

1. Introduction

Total dissolved solids (TDS) and total suspended solids (TSS) are two physical water quality parameters (WQPs) that impair the quality of water resources such as rivers and lakes [1–3]. Both TDS and TSS are fractional constituents of "total solids" of the same sample separated by filtration [4]. Total solids refers to "the material residue left in the vessel after evaporation of a sample and its subsequent drying in an oven at a defined temperature" [5].

The 23rd edition of the American Public Health Association Standard Methods for the Examination of Water and Wastewater, Section 2540 defines TDS as constituents of total solids in a water sample, which passes through 2.0 μm or less nominal pore size under specific conditions. Constituents of TSS in any given sample of water are retained by a filter with a 2 μm or less pore size measured by weighing the dried residue left on the filter [4,5]. Constituents of TSS encompass particulate matter including sediment, silts, and algae among other solid suspended particles. TSS, however, does not include colored dissolved organic matter (CDOM). The presence of these CDOM, phytoplankton, and non-algal particles (NAP) at various compositions often poses a challenge to the determination of WQPs such as TSS [2,6].

Increased concentrations of TDS and TSS in water bodies limit them from serving their purpose for drinking, power generation, industrial cooling, supporting biodiversity, ecosystem services, recreation, transportation routes, waste disposal, agriculture production, irrigation, energy production, regional planning, and fish farming [7–17]. Impairment of water bodies by parameters such as TDS and TSS is caused by climate change, development, and urbanization associated with surface imperviousness resulting from increased population, and contamination caused by rapid and uncontrolled environmental changes including drought, wastewater discharges, nutrient pollution, sediments, and changes in land use and land cover which results in negative impacts such as the proliferation of harmful blue-green algae, accelerated eutrophication, and extreme turbidity among others which have negative implications on the sustainability of the limited water resources [3,6,18–29].

Changes in the quality of water resources by these parameters can cause changes in the quality of recreational and commercial activities. There is a decline in boating, fishing, and swimming in these water bodies when they are impaired, which brings about significant economic losses. Swimming and boating in impaired water may also result in respiratory and gastrointestinal diseases [30,31]. A study performed through the use of biophysical modeling established that Virginia households are ready to pay as much as USD 184 million yearly to ensure there is an improvement in the quality of their water [31].

To protect and restore the quality of water resources, monitoring efforts and management strategies are key and need to be successful to achieve the desired results of a healthy water body in the ecosystem economy [32,33]. Monitoring and assessment of WQPs such as TDS and TSS are crucial to fully comprehending how changes in the natural environment and human activity affect water bodies [34]. TDS and TSS have been widely monitored using conventional or traditional methods such as laboratory analysis or grab sampling [2,19,35], these methods are, however, time-consuming, expensive, and need a lot of labor. As a prospective alternative to traditional methods for measuring TDS and TSS, remote sensing (RS) techniques have gained popularity in recent years and have proven to be cost-effective in monitoring these WQPs on local to global spatiotemporal scales non-intrusively [2,36,37].

Although TDS is not regarded as a principal water pollutant, it is an indicator of water quality. High concentrations of dissolved solids may significantly affect the palatability of drinking water. In addition, high TDS levels can cause scaling and corrosion in cooling water and boilers. TDS in water originates from irrigation returns, urban runoff, natural sources, municipal, road deicing, industrial waste, chemicals used in water treatment, and the actual plumbing infrastructure [38,39]. Drinking water with high concentrations of dissolved solids may affect the taste of the water. In addition, high TDS levels can cause scaling and corrosion in any application, particularly in cooling water and boilers, and therefore need to be monitored in water systems [38]. TSS also needs to be measured, monitored and managed because the performance of filtration systems, plumbing systems, and capital equipment can all be impacted by high amounts of suspended particles in water. Quantification of TSS is needed to design dredging plans for navigational channels and estimate the fluvial solid discharges to water bodies [40]. Additionally, high levels of suspended particles in rivers, streams, lakes, and reservoirs can disrupt the natural ecology of these water systems. Monitoring of TSS in the water is therefore essential to preserve the general well-being of the water bodies [38].

This paper, therefore, provides an overview of different methods used in the measurement of TDS and TSS or sediment concentration from the perspective of conventional and RS approaches. In this paper, we examine the advantages and limitations of each technique along with how RS multispectral and hyperspectral images can enhance remotely sensed estimations of TSS and TDS. In addition to highlighting the potential of RS techniques for enhancing our knowledge of water quality, the purpose of this study is to present a thorough and concise state-of-the-art summary of the approaches used in TDS and TSS assessment. The findings of this study can aid in the development of novel TDS and TSS monitoring techniques as well as increase the effectiveness and precision of water quality monitoring efforts.

While conventional methods have been used to monitor WQPs such as TDS and TSS, the use of RS has recently emerged as an alternative force in the monitoring of particularly optically active TSS largely because it can be optically sensed by sensors. Measurements of optically inactive TDS are due to their association with other colored WQPs with which they may co-vary [2,36,37,41]. Despite the significance of monitoring TDS and TSS levels in water bodies, there hasn't been much research published that has compared traditional and RS methods in great depth. Analysis of these previous reports presents an opportunity to provide an overview of a published journal that highlights the advanced RS applications in monitoring these specific WQPs.

The novelty of this research consists of providing an integrated review of both conventional and RS applications in the monitoring of TDS and TSS. This study offers a thorough analysis that integrates the benefits and drawbacks of both methodologies, in contrast to earlier review studies that frequently concentrated mainly on RS techniques. This study, therefore, provides a broad and exhaustive understanding of the dynamics and impact of these WQPs in water bodies.

This study also provides insights into microwave sensors utilized in the monitoring of these WQPs. Additionally, most review studies on WQPs focus on a general application of RS techniques on WQPs without specifically highlighting the advanced RS platforms and sensors, and the pros, and cons of multi and hyperspectral images in estimating these key WQPs. Furthermore, there are hardly any previous literature reviews that have offered a comprehensive assessment of traditional techniques for determining TDS and TSS levels and the impacts of increased levels of these WQPs on the sustenance of aquatic and human lives. Most of the information on conventional methods for determining TDS and TSS levels is instead found in reports and other unreviewed sources.

This study, therefore, focuses on providing a comprehensive review of monitoring these WQPs in water bodies by synthesizing the available data from both journal papers and non-peer-reviewed sources. We seek to give a thorough review for monitoring TDS and TSS levels in water bodies. We do this to bridge the information gap between the body of published literature and the quantity of information contained in reports and to offer academics and practitioners interested in monitoring these parameters a comprehensive repository.

2. Search Engines and Overview of Parameters

The literature review encompasses searching and navigating through several databases in the English Language including the Web of Science™, Google Scholar™, Scopus™, ResearchGate (RG), Semantic Scholar™, and Multidisciplinary Digital Publishing Institute (MDPI) using keywords such as remote sensing, satellite, total dissolved solids, total suspended solids, sediments, salinity, water quality, machine learning, and or different combinations of these keywords [27]. Additionally, we searched and included other related journals of importance. Searches were also performed for reports and important information relating to the subject from Government web pages including the Bureau of Reclamation, National Aeronautics and Space Administration, and the United States

Environmental Protection Agency among others. We also searched the American Society of Civil Engineers Libraries for related works published in the Environmental and Water Resources Institute conference proceedings. Additionally, we searched through Google for related reports and web pages of brands and companies containing information on the measurement of TDS and TSS. Searches of articles and reports generated a total of over 1000 published works across the globe. These articles, proceedings, reports, and web information were screened to only return articles, reports, and web information of relevance to the TDS and TSS estimations with conventional and remote sensing methods and other related materials of significant importance all totaling close to 280 works from the 1980s to 2023 as used in this study. The approach used in the literature search is depicted in Figure 1.

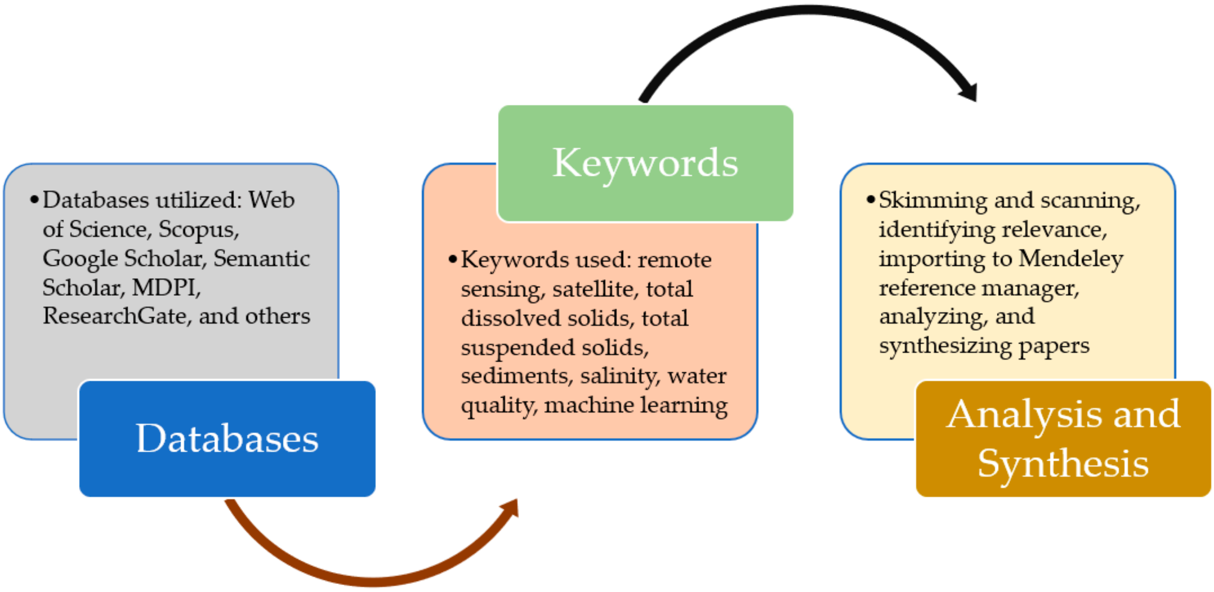

Figure 1. Schematic approach for literature search.

The findings and the overview of the studied parameters are presented in the following subsections.

2.1. Overview of TDS and TSS

TDS and TSS concentrations are issues of great concern as they impact the quality of water. Finding ways to reduce the devastating effects of salinity and sediment concentrations in water bodies is necessary to protect water resources and biodiversity.

2.1.1. Overview of TDS

TDS includes materials that due to their small size, pass through filters during water analysis [4,5], including dissolved ionic constituents such as Mg^{2+}, Ca^{2+}, Na^{+}, and Cl^{-}. These ions pose challenges in drinking water and wastewater treatment systems since they are not removed through various mechanical treatment methods [3,42]. TDS and salinity are defined differently [43]. TDS is a measurement of the mass of filterable dissolved organic and inorganic substances per unit volume remaining from the evaporation of water [43]. Salinity measures the mass of dissolved salts in a known mass of solution [4,43–46]. TDS can be about the same as salinity in clean water [47]. Higher TDS concentrations in water mean increased conductivity and may also mean decreased dissolved oxygen [48]. TDS is composed of salts, metalloids, metals, and dissolved organic matter. Organically derived TDS is generated by the release of organic molecules during the growth and decay of biological matter, such as roots and microbes in streams. Other contributing factors to TDS in streams include soil or sediment minerals' dissolution, desorption of ions linked to solids, and atmospheric precipitation. Chemical and biological processes including temperature, dissolved oxygen concentration, pH, organic carbon, and rock decomposition impact these contributing factors [49]. Temperature increases intensify stream drying and cause a rise in TDS concentration [50]. The types of mineral and their abundance in water strongly impacts the quality of the water [51]. The United States Environmental Protection Agency (US EPA) has listed TDS in its secondary drinking water regulations (SDWR) with the allowable TDS limit in water set to 500 mg/L. SDWRs are non-enforceable federal guidelines that cause aesthetic or cosmetic effects. Examples of cosmetic effects include taste, color, or odor while cosmetic effects include skin or tooth discoloration [52–54].

According to [55], TDS above 1200 mg/L is inappropriate for potable consumption. Depending on the amount of TDS in water bodies, they may be classified as brackish water or saline water. brackish water has a TDS varying from 400 to 1000 to about 10,000 mg/L [56,57]. Saline or salt water has a TDS concentration of more than 10,000 ppm. Oceanic salinities typically vary from about 31 to 36 ppt [58,59]. Brines are defined as waters with salinity greater than 35,000 mg/L [60,61].

Studies conducted to assess the effects of TDS on the performance of lactating dairy cattle show varying results on water and feed intake and milk production. An increase in TDS concentration is associated with a more likely decline in milk production in cattle during the summer season. While some researchers found a decline in milk production during heat stress in cows given water with TDS concentrations of 4300 ppm others found no effect on milk production of cows given water with 3500 ppm TDS concentrations. Interestingly, other researchers suggested that desalination of water reduced TDS from 14,000 to 400 ppm and thus increased the milk production of high-yield dairy cattle experiencing heat stress [62].

2.1.2. Overview of TSS

TSS may include a large fraction of mineral seston derived directly from terrigenous sources or indirectly by resuspension of already deposited materials. It is an optically active parameter often referred to as suspended sediment concentration (SSC) and plays a critical role in the management of water resources as they are linked with the fluxes of water contaminants, namely micro-pollutants and heavy metals [7,46,49,63,64], and is a key variable used to describe and control sedimentation dynamics in water bodies [65]. Mineral extraction and energy resources are contributing factors to the increase in TSS in water bodies. Mining activities reported to increase the TSS in a particular water body include mine site preparation, crushing, and storage of materials that are often exposed or aggravated by precipitation or rainfall events [49].

TSS and its many forms of occurrence such as suspended particulate matter (SPM), total suspended matter (TSM), suspended solids/sediments (SS), and SSC are an integral part of the geochemical, global geological, and biological cycles in the aquatic environment due to their ubiquitous nature, mobility, and underlying physiochemical properties [66].

TSS or SSC is the most common water pollutant by weight and volume in inland surface waters [67]. TSS and SSC are often used interchangeably. The only difference between TSS and SSC is the laboratory analyses used for their assessment [44]. Sediment transport in the water bodies is a source of pollutants such as nitrate, metals, carbon, and many others in the water [68]. TSS may be composed of sand, mineral precipitates, biological materials, silt, and clay and its formation is influenced by physical processes largely controlled by hydrology. Some of these physical processes include the aggregation of dissolved organic materials, erosion of stream banks, and surface soils [49,50]. There is a range of sediment criteria in the US depending on the state. While some states use numerical criteria, others use narrative criteria, some also utilize the numerical and narrative approach, and some have no criteria at all for suspended and bedded sediments (SABS). SSC concentration is limited to 30 to 158 mg/L for the few states that use suspended sediment as a criterion [69].

3. TDS and TSS Related Issues

3.1. TDS Issues and Implications

TDS concentrations in water bodies are an important parameter for consideration as it contributes to the cost involved in the desalination treatment of water. Researchers in [70] classified desalination methods for the treatment of water into two, namely phase change processes or thermal methods and single phase or membrane processes. Examples of thermal methods include multi-effect distillation (MED), vapor compression (VC), and multistage flash (MSF). An example of the membrane process method is reverse osmosis (RO). The thermal methods are, however, said to be more effective approaches than the membrane methods in terms of efficiency in the desalination of seawater with much higher salt contents. The higher the amount of TDS concentration in the water, the greater amount of pressure required for the pumps to push water through the membranes in RO systems which consequently increases the cost of energy [71]. The unit cost of RO systems ranged from USD 0.32 to USD 0.44 per m^3 for brackish water while that of seawater ranged from USD 1.57 to USD 3.55 per m^3 in 1988 as reported by the US Congress. The cost of desalinating 2300 ppm of Jordan brackish water is reported as USD 0.26 per m^3, while brackish water in Florida of 5000 ppm costs USD 0.27 per m^3, an indication of the different costs associated with desalination systems of different concentrations, locations, and energy sources or technologies used [70].

Salinity exists in the concentration of mineral salts in soils or water, and it occurs through natural processes including storm surges, floods, and poor management practices. Salinity intrusion is an issue of great concern, particularly in coastal regions worldwide. Salinity intrusion impacts agricultural activities. Issues of salinity affect the natural environment and are a major cause of economic loss due to their devastating effect on agricultural productivity and food safety. These issues are likely to be aggravated due to climate change coupled with the rise in sea level and human activities such as agricultural runoff, untreated sewage discharges, vegetation clearance, irrigation, regulation of river hydrology, application of road deicing salts, and mining [7,49,72,73]. The World Bank Group 2018 estimated that about 6–12 million people are likely to be impacted by coastal flooding by 2070–2100 with climate change also expected to cause a reduction in national income by approximately 3.5% by the year 2050 [73]. Salinity reduces the osmotic potential, making it strenuous for plants to extract water causing toxicity of specific ions, nutritional imbalance, and affecting the permeability and tilth of the soil. This subsequently resulted in the reduction of crop yields [74].

Salinization of a freshwater ecosystem is a common environmental issue of global concern. It is predicted to impact more than 7000 lakes in the Midwest and Northeast US [72,75]. One of the fast-growing causes of salinity in freshwater systems in Europe is the use of road deicing salts. Salt concentration in Lake Constance, the second largest freshwater lake by volume in Europe, is said to have more than doubled, with salt concentration accounting for 52% of the elevated salinization. Road deicing salts are largely used on the road during dangerous winter conditions to increase the safety of humans traveling on the roads. Road deicing salts have been found to reduce on average 87% and 78% of accidents on two-lane and multi-lane highways, an indication of their immerse contribution to reducing road crashes. These salts, however, dissolve and find their way into the freshwater ecosystems through saline overland flows produced by snowmelt, rain, and groundwater sources [72].

Salinity intrusion in water bodies occurs when salts get dissolved and accumulated in the water bodies at a rate that impacts agricultural production, the environment, and the economy. Salinity has the potential to affect the metabolism processes of aquatic organisms, threatening the lives of these organisms [73]. Salinity affects the biological process in ecosystems causing deterioration in the quality and the health of soil and water resources. Issues relating to salinity are severe in arid and semi-arid regions [76]. Salinization is primarily caused by natural processes such as a flood, or storm surge. These processes are aided by climate change which afflicts more than 20% of the world's agricultural regions. Secondary causes of salinization are largely due to anthropogenic activities [77,78]. Anthropogenic activities including agricultural runoff, the use of fertilizers, wastewater treatment discharge, and road salt application greatly alter the natural concentrations of salt in inland waters contributing to freshwater salinization, a phenomenon faced by thousands of water bodies worldwide in the last few decades [75,77,78]. Salinization in water bodies results in high chloride concentration which has the potential to lead to the corrosion of water distribution systems leading to the release of lead and copper into drinking water supplies [75]. Basic sources of salinity include discharge from wastewater treatment plants, nonpoint source discharges such as agricultural runoff, and leaching of soil [79].

Salt loading in lakes may be a contributing factor to the shifting timing of lake stratification and spring mixings of lakes. An increase in salt concentration not only poses a danger to freshwater organisms but can also cause stabilization in water columns due to the density difference between less dense fresh and denser saline water. Salinization is also a major hindrance to an ecologically significant spring turnover event of water columns. Lake salinization can potentially impact the stratification and mixing of the lake as the density of the lake profile is influenced by the mixing dynamics of the lake. The buildup of salt concentration in lakes can cause a corresponding increment in density gradients in the column of water which could delay, diminish, and or disrupt lake mixing. The effect of temperature on the density of freshwater lakes largely influences their stratification [75].

In the study [75], to assess the impact of salinization on lake stratification and spring mixing, the impact of salinization on mixing in Lakes Mendota and Monona located in Wisconsin was investigated by using an analytical approach to quantify salinity thresholds and the long-term impact of winter salt loading on mixing and stratification. It was established that increases in water loading causes a delay in spring turnover, prolonging summer stratification, and increasing water column stability in northern temperate lakes. Lake mixing is also influenced by water density which is induced by salinity [80].

The quantified economic damage due to excessive salinity in the Colorado River Basin (CRB) was reported to be USD 295 million in 2010, with agriculture getting hit the most with USD 153 million in damages representing 52%, followed by households with a value of USD 83 million representing 28%. Commercial and management came next with each representing 6%, followed by utility and industries having a lesser impact of 4% each [81]. Other studies have reported the annual economic damages to be over USD 300 million [82]. The effect of the salinity in the CRB is a major issue for both the US and the Republic of Mexico since both countries rely on the river for water. Salinity issues cause adverse effects on millions of acres of irrigated farms and the people who depend on the river for water [81,83]. It is also a priority to ensure compliance with the 1944 Treaty signed between the United States (USA) and the Republic of Mexico, which limits the TDS concentration in the approximately 1.850 km^3 discharge to the Republic of Mexico annually [79,82,84]. The US–Mexico Water Treaty is a complex, multi-basined transboundary water diplomacy that is focused on water allocation critical to each of the two country's water security in the border region. The treaty is said to be the single most important bilateral agreement on water resources between the two countries and not only is it durable, but is also shown to apply to environmental challenges which were unforeseeable to the drafters [85]. The salinity in water bodies may be influenced by changes in streamflow, reservoir storage, and natural variations in salinity, water use by municipal and industrial players, as well as agricultural practices and energy development such as coal, oil, and gas. An increase in streamflow dilutes the salinity in water. Salinity is increased when the flow levels decline (at high evaporation) and reduce at an increased level of flow (i.e., when evaporation is less). Climatic changes in rainfall and snowmelt runoff play a significant role in the differences in inflow and salinity. Reservoir storage alters the salinity variability of downstream rivers. Large reservoirs selectively route less saline water but hold more saline water during the period with low flows. Poor water quality is subsequently relieved when inflows begin to increase. Irrigation activities are the largest contributor to salinity in the CRB. Irrigation causes an increase in the salt concentration of the source water by consuming water through evapotranspiration and leaching salts found in saline soil and geologic formations [18,81,86]. Irrigation is said to have contributed about 661,000 megagrams of salinity load annually to the upper CRB (UCRB). Excessively exposed bare ground in mountainous areas is reported as a source of salinity contribution to the UCRB [45]. A study by [87] to assess the TDS contribution to the Colorado River due to population growth in the Las Vegas Valley using system dynamic models revealed that the TDS concentration in the Las Vegas Wash will rise to about 14% in the year 2035. A 10% reduction in population of water softeners users by 2035 will also cause a reduction of TDS level by 126 mg/L.

3.2. TSS Issues and Implications

The US EPA identifies fluvial sediments as the most pervasive pollutant in the rivers and streams of the US, impacting aquatic habitat, drinking water treatment procedures, and recreational usage of rivers, lakes, and estuaries [88]. The US EPA in their 2017 National Water Quality Inventory Report to Congress cited sediments as one of the leading causes of impairment in the water bodies assessed. The report revealed that 15% of river's and stream's lengths have excess streambed sediments which were found to have quite an impact on the biological conditions of the water bodies [89].

Suspended sediments in water may not be toxic, but an excessive amount leads to a high level of turbidity. Turbidity is a visual characteristic of the water consisting of biotic and abiotic elements that indicate its clarity or lack of it due to the presence of organic and inorganic suspended materials or matter (SM), plankton, and microscopic organisms causing scattering and absorbing of light [4,28,90,91]. Turbidity in water could be measured conventionally in the laboratory through the nephelometric method and by measurements using optical in situ sensors often called turbidimeters as described in Section 2130B and 2130A, respectively, of the standard methods for the examination of water and wastewater [4]. Turbidity and turbid waters have also been studied and monitored using RS images [92–96]. Researchers found satellite-derived reflectance from the National Aeronautics and Space Administration (NASA)'s Moderate Resolution Imaging Spectroradiometer (MODIS) at the wavelength of 667 nm to be a proxy for water turbidity measurements, with larger values of water turbidity resulting in higher reflectance at 667 nm wavelength [92].

Turbidity is increased during the period of high flow events due to increased concentrations of sediments making turbidity a known surrogate or proxy for TSS concentration [28,94,97]. Studies have also estimated turbidity from forms of TSS in water bodies using empirical relationships [94,98]. Researchers found a high correlation of 0.986 between TSM and turbidity in the Southern North Sea, UK [98]. Other researchers in [99] also found an almost perfect correlation (r = 0.99) between turbidity and TSM concentration following the removal of outliers in the data in the brackish lower sea Scheldt, located at the border of Belgium and the Netherlands. Another study by [100] also found a correlation of 0.91 between turbidity and SPM in the Río de la Plata estuary in South America which is widely known to be among the most highly turbid rivers worldwide with TSM concentrations of 100–300 mg/L [101].

A high water turbidity index, as a result, causes a greater amount of scattered light in several directions, which further leads to a reduction in light penetration deep into the water bodies and consequently impacts the rate of photosynthesis, leading to oxygen depletion. The high amount of TSS concentrations can raise water temperatures and lead to lower dissolved oxygen concentrations. Because the suspended particles absorb more heat and use up more oxygen, the water may heat more quickly as a result, which may be harmful to aquatic life [38]. TSS can also cause clogging in the gills of fish leading to their death [49,102–104]. The reported average upper tolerance level of SSC is about 90 mg/L for fish and 13 mg/L for bottom invertebrates [69]. These conditions are about twice as likely to occur in streams and rivers with high levels of streambed sediments than in those without. Sediments in the water can result in smoother streams causing suffocation of fish eggs and organisms dwelling in the bottom water. Increased sediments in the water can also interfere with recreational uses and drinking water treatment processes [89].

Sedimentation is a key issue in the sustainable management of water supply systems. Accumulation of sediments is a likely phenomenon in lakes and would therefore need to be addressed since it impacts the quality of water [105]. It is important to understand issues relating to sediment concentrations that impact the quality of water and subsequently affect human and aquatic life that depend on the lake as their source of water. SS affects the optical clarity of the water. TSS causes the scattering of light and impacts the optical properties of water. Detection of these particles in water using RS or UV systems is possible since they cause scattering of light [106]. The higher the TSS concentration in water, the harder it is for light to travel through the water creating turbidity. Turbidity is said to correlate with TSS. The higher the amount of TSS in water, the more turbid the water appears. TSS is an important parameter for consideration because it impacts the amount of sunlight penetration to the water body which subsequently negatively impacts photosynthesis needed for the growth of plankton and algae [7,36].

A study performed by [107] found a significant correlation between SS and turbidity. For a sample size of 19, the reported coefficient of determination (R^2) in the study was 80%. The presence of sediments in water is said to cause turbidity which settles on the floor of the water reservoir. Reservoirs have a known volume of water storage capacity at the time of inception. This however reduces with the siltation mechanism [108].

Researchers in [102] found a possible impact of years of drought on the rise in the concentration of TSS in the Overton and Colorado River Arm of Lake Mead located in the Western US, specifically in Las Vegas, Nevada. Lake Mead is the largest reservoir in terms of water capacity in the US and the 16th worldwide. An estimated 98% of the Lake's inflow is said to be from the Colorado River, which is a conduit of sediment transport from the UCRB. This sediment transport into the Lake has seen a 90% reduction since 1963 when the Glen Canyon Dam was completed. Despite these efforts in reducing sedimentations, the need to assess the impact of TSS is crucial in achieving desired results in water resources management efforts [102].

4. Measurement and Monitoring of TDS and TSS

TDS and TSS have traditionally been analyzed and monitored through field or in situ sampling and laboratory testing generally classified as conventional methods. Field and laboratory measurements include grab sampling, filtering, and evaporating a sample through a fine filter paper followed by drying in an air oven which are collectively known as gravimetric methods [35,109]. Conventional methods of monitoring of WQPs are, however, cost-prohibitive, labor-intensive, time-consuming, and, also not suitable for large-scale analysis [46,103,110,111].

4.1. Measuring TDS and TSS Using Conventional Approaches

Several techniques and tools are used to measure TDS or TSS in a lab or out in the field. TDS and TSS can be measured using the US EPA Gravimetric method, and direct measurements as set by Sections 2540C (for TDS) and 2540D (for TSS) of the Standard Methods for the Examination of Water and Wastewater [4]. The various conventional approaches used in the quantification of TDS and TSS are described in Sections 4.1.1 and 4.1.2.

4.1.1. Measurement of TDS

TDS or dissolved solids (DS) concentration is measured either directly or indirectly.

Direct TDS determination involves grab sampling which entails the collection of individual samples at specified times which are reflective of the water conditions at the moment the sample is collected [35]. These samples are prepared in the lab and oven-dried. TDS is then determined by weighing the residue that remains after the evaporation of a specific volume of a filtrate. TDS can also be analyzed in the field or lab by utilizing electrochemistry meters and probes developed to detect the dissolved solids in a sample [38].

One way to indirectly determine TDS involves the summing of measured concentrations of various constituents in the filtered water sample. Researchers in [112] have found strong correlations among various dissolved minerals such as TDS, electrical conductivity (EC), and chloride with r > 0.8 which makes the EC an effective tool for determining the salinity of water [113]. TDS can therefore be estimated indirectly by multiplying EC measured in micromhos per centimeter by an empirical factor that ranges from 0.55 to 0.9. The exact factor used in TDS estimation is influenced by the temperature and soluble components of the water which is determined by establishing repeated paired linear regressions of measurements of TDS and specific conductance for a specific water body. A high factor is used for saline water while a lower value is used for water systems with considerable hydroxide or free acid [4]. A value of 0.67 is often adopted for several natural water systems [4]. However, Ref. [114] used a correlation factor of 0.64 in their study to estimate and characterize physical and organic chemical indicators of water quality. Both TDS and EC are used to describe the salinity level in the water. EC measures the capacity of the water to conduct an electric charge and its ability to do so is influenced by the ionic strength, temperature of measurement, and concentrations of dissolved ions. The concentrations of these dissolved ions are measured as TDS. TDS analysis is said to offer a better understanding of groundwater quality and the effect of seawater intrusion compared with EC analysis. While the EC of water is inexpensive to measure and can be measured in situ through the use of a portable water quality checker, analysis and measurement of TDS are, however, more difficult, time-consuming, and expensive [109]. TDS estimation from EC using a correlation factor is based on the assumption that dissolved solids are mainly ionic species of low concentration needed to yield a linear EC–TDS relationship [115]. Chemical analysis is said to be the only reliable means to measure TDS. This method can, however, be time-consuming and costly. An indirect method is usually used to aid in the effort of salinity measurement. The direct method is performed through the measurement and establishment of empirical relationships between salinity and other physical properties of water such as conductivity, sound speed, refractive index, and density [4].

4.1.2. Measurement of TSS

Several researchers have monitored TSS in water bodies because it is key to ensuring the restoration of the integrity of water bodies, leading to the sustainability of water resources and ultimately protecting human and aquatic lives [116,117].

Water loaded with suspended sediments increases its turbidity, reducing its light absorption capability while allowing a greater amount of reflection. An increase in sediments and turbidity, therefore, causes an increase in the reflectance of light in the visible and the near-infrared (NIR) spectrum of the electromagnetic spectrum [46]. The remotely sensed estimation of sediment concentration (TSS) is influenced by particle parameters, including their size, shape, density, and color, dissolved and particulate color. Suspended particles originate from runoff, soil erosion, stirred bottom sediments, algal blooms, or discharges. The composition of TSS materials in inland waters includes components supplied by tributaries called allochthonous and components produced within the water column called autochthonous and resuspension [118]. Both TSS and turbidity are used as indicators to assess the clarity of water and are a macro-descriptor for water quality as they are directly related to other variables used in the management of inland waters such as the lake. The composition of suspended particles may differ in inland waters as they are governed by characteristics of the drainage basin, resuspension of bottom deposits driven by motion, and hydrology [118].

Researchers in [119] found a correlation between TSS and turbidity of 0.64. A sampling of TSS can be performed using multiple particle filtration systems (MuPFiSs), a system that has four filtration lines in parallel with water meters to measure the flow of water filtered over a period under pressure using appropriate filter pore sizes [120]. In a study performed by [121] to analyze WQPs including TSS in the effluent of a WWTP in Switzerland, an in situ UV spectrometer was applied to the effluent and calibrated using a multivariate calibration algorithm and partial least squares (PLS) regression. The accuracy of the TSS measurement was found to be unsatisfactory. This is because the spectrometer used did not cover a wavelength spectrum of up to 700 nm, which was said to give a better signal for TSS calibration owing to the strong correlation between TSS and turbidity.

Researchers in [122] estimated TSS concentrations using ML models coupled with several watershed factors rainfall depth, drainage area, percent of imperviousness, runoff volume, land use, and antecedent dry days for various storm events retrieved from 17 US states. The authors reported they found the random forest and the adaptive boosting regressors the best models for TSS estimations from these watershed factors with $R^2 \geq 0.64$ and Nash–Sutcliffe Efficiency (NSE) ≥ 0.62 from the training to the prediction steps of the models.

4.1.3. Strengths and Limitations of the Conventional Method for Measuring TDS and TSS

The strengths and limitations associated with the conventional methods of measuring TDS and TSS in water bodies are introduced in Table 1 [2,4,36,38,123,124].

Table 1. Strengths and limitations of conventional methods for measuring TDS and TSS.

Strengths	Limitations
Well-established standardized methods	Labor and cost intensive and time-consuming
Associated with a high degree of precision and accuracy	Accuracy may be impacted by errors associated with field samplings, transportation, storage, and lab analysis
Can provide WQP measurements at varying depth	Impossible to monitor the entire water body at the same time due to inaccessibility issues due to topography
Does not involve the knowledge of big data processing and the complexity of data analysis	Knowledge of specialized measuring devices or equipment may be required
Provides direct measurement of WQPs	Limited spatial and temporal coverages

The following paragraphs further explain the strengths and drawbacks of conventional methods of measuring TDS and TSS.

Strengths

Conventional methods [38], are well-established methods employed in laboratories and have been used for decades. They have been proven to produce reliable and accurate results and are widely understood by many experts and researchers in the field of water quality and water resources management.

There is a substantial body of literature on the subject in terms of reports provided by governmental and non-governmental institutions and companies [4,38,88,123].

Conventional methods also present details about instantaneous concentrations of TDS and TSS at a certain time. Additionally, conventional methods present standardized procedures for determining TDS and TSS which means the results from different measurements can be compared [4,35].

Limitations

Conventional methods of TDS and TSS measurement techniques can take a lot of preparation and analysis time. From sample preparation to oven drying in the case of TDS measurements, the conventional method requires significant time ranges from hours to days for their analysis [125]. The time required to collect samples, send them to a laboratory for processing, and receive findings can be long and particularly cumbersome when sampling at multiple locations [126].

Conventional methods of TDS and TSS measurement techniques can be laborious and require skilled personnel for effective and accurate measurements, analysis, and interpretation of results [125].

Some standard or conventional methods of measuring these WQPs require the use of dangerous chemicals and specialized equipment which can pose safety issues to researchers and laboratory technicians [4,125].

Conventional methods are limited by spatial and temporal resolution. Traditional approaches require physical sampling and are therefore confined to using the point measurements taken at certain times and locations, which may miss significant changes in water quality across time and space and are therefore not feasible for large or remote water systems [2,36,127–129].

4.2. Monitoring of TDS and TSS Using RS

This subsection presents the sensors used in monitoring TDS and TSS as well as the principles and methods used in the retrieval of these WQPs.

4.2.1. Concept of TDS and TSS Interactions and Measurements Using RS

The basic underlying principle and concept of retrieving WQPs such as TSS and TDS from RS are based on the interaction of suspended and dissolved colored substances with light. Dissolved colored and suspended substances increase light absorption (dissolved) and absorption and scattering (suspended) in water and change the direction of the returned light. The spectral distribution of backscattered energy is affected by additional absorption by dissolved colored matter in the water column. SM on the other hand increases the backscattering of light and hence may increase the remote signal [130]. The interaction of light with SM produces a signal reflectance that is detectable from a distance. These signals can therefore be used to estimate the presence and the quantity of TSS. The strong backscattering property of TSS makes it possible to be detected by RS techniques [131]. The spectral properties of the water are categorized as the Inherent Optical Properties (IOPs) and the Apparent Optical Properties (AOPs). The IOPs which describe the spectral light absorption and backscattering are key components in linking reflectance measurements to the concentrations of water parameters such as TSS. The absorption coefficients of particles in optically complex waters such as inland, coastal, and estuarine are broken into components caused by phytoplankton and those caused by non-algal particles. While the IOPs can be quantified in the laboratory, the AOPs which include radiance and downwelling plane irradiance are only measured using the IOPs and depend on the IOPs and the geometric structure of the radiance distribution including the wind speed, surface water structure, and atmospheric conditions [118,132].

RS-based approaches for the estimation and retrieval of the TSS and TDS involve establishing relations between these WQPs and spectral properties of RS images. The approaches include empirical methods which utilize statistical relationships derived from measured RS spectral properties and these WQPs. These are simple and straightforward approaches which been used in the effective estimation and retrieval of these WQPs [10,41,124,133–137].

Another approach used is the analytical method which uses the IOPs including the scattering and absorption coefficient and the volume scattering function, and the AOPs such as the diffuse attenuation coefficient for downwelling irradiance and the irradiance reflectance to model and derive these WQPs [2,124,133,135]. Other studies are semi-empirical methods: which are a combination of the empirical and analytical methods for the retrieval of these WQPs [2,10,124,133,138–140]. In this approach, the spectral radiance is recalculated to above the surface irradiance reflectance and subsequently, through regression techniques related to the TDS and TSS. Over the years, studies have developed and improved these approaches leading to more recent use in the state-of-art artificial intelligence (AI) approaches such as machine learning (ML) models and deep learning which uses implicit algorithms to capture both linear and nonlinear relationships compared with the conventional statistical methods [2,124,141–145].

4.2.2. Optical Characterization of TDS and TSS

WQPs are categorized as optically active and inactive parameters for RS applications. Optical RS is based on the difference in spectral reflectance of water and land [146]. Optically active water parameters are those parameters that are likely to impact the optical characteristics measured by RS sensors while non-optically active parameters are those parameters that are less likely to influence the optical characteristics measured by the RS sensors [147]. TSS is an optically active parameter while TDS is an optically weak property. Optically active parameters such as TSS absorb light in the ultraviolet and visible wavelength range and influence the optical properties enabling them to be sensed from satellite observations. Optically active water parameters are also used to monitor several other processes aside from water quality. The high amount of sediment loads have the potential to reduce water clarity and block radiation needed for submerged aquatic vegetation growth. Sediments affect the optical characteristics of estuarine waters making a color in both in situ and RS a good indicator for monitoring phenomena, including run-off processes [148]. Studies have also found a good correlation between the SPM concentrations and water reflectance in the green and red regions of the electromagnetic spectrum for low to moderately turbid waters [138]. The reflectance in the 580–680 nm and 700–900 nm ranges of the electromagnetic spectrum have been reported to be most sensitive to TSM concentration changes and hence most ideal for the retrieval of TSM concentrations [124]. A study by [149,150] corroborated this assertion by finding SS concentration to be associated with an increase in reflected energy at longer wavelengths (630–690 nm).

A study was performed by [151] to estimate optical water parameters using a guided approach. The optical WQPs considered included TSM using the Ocean and Land Color Instrument (OLCI), and MSI data at Estonian and Finnish lakes and the Baltic Sea coastal area. The study used empirical algorithms. A high correlation ($r > 0.87$) was established for in situ measured optical WQPs and the parameters predicted by the optical water-type guided approach. The amount of SSC and turbidity affects the reflectance of light with the relationship between spectral reflectance and SSC or turbidity often described as a positive linear correlation or nonlinear regression in the visible and the NIR wavelengths [152,153].

Researchers [154] found an increase in reflectance in the NIR regions and reduced reflectance in red and SWIR due to high water absorption in the most turbid regions of the Río de la Plata estuary located in South America. Researchers [155], however, noted the NIR spectral bands to be less sensitive to the increase in TSM concentrations in highly turbid waters with TSM > 100 mg/L making the use of SWIR with a wavelength of 1000–1300 nm an alternative in such scenarios.

Studies have also found a relationship between the optimum wavelength and the SSC and have therefore developed empirical relationships between the SSC and reflectance radiance for a specific site and date [67]. TDS and other inactive optical parameters are measured owing to their correlations with optically active parameters. Studies performed have also measured the correlations between WQPs such as in the case of optically active and optically inactive parameters which would be useful in the case of determining TDS. For example; researchers in [156] found a moderate correlation of 0.435 between TSS and TDS for the study to map WQPs using Landsat 7 ETM+ for Manzala Lagoon, Egypt. The study also found a moderate correlation of 0.43 between the band ratio (B2/B4). Researchers in [157] also developed a correlation matrix for both optical and non-optical WQPs. Correlation between TDS and TSS, TDS, and turbidity were reported as 0.35 and 0.58, respectively. Although TDS is not spectrally active, it can be estimated from RS using various models including the semi-empirical models. Retrieving optically inactive parameters such as TDS using satellite visible, NIR, or IR bands is possible because of the assumption that they may be highly correlated with optically active parameters and assuming that there is some process that (usually) co-occurs with changes in the TDS or salinity that are affecting a WQP that is optically active. These processes may, however, not always co-occur at the same magnitude.

4.2.3. RS Sensors for Monitoring TDS and TSS

Microwave and optical RS technologies are two technologies used in the estimation of WQPs including TDS and TSS. Optical RS sensors collect data in the visible, near-infrared, and shortwave infrared regions of the electromagnetic spectrum, but microwave sensors use a longer wavelength (cm to m) which makes them able to penetrate through cloud cover, dust, haze, and all kinds of rainfall except the heaviest rains. The longer wavelengths of microwave sensors make them insusceptible to atmospheric scattering which impacts shorter optical wavelengths which makes it possible for them to detect microwave energy under all weather and environmental conditions at any time [158–160]. Microwave sensors provide cost-effective, reusable, reliable, and automatic water-sensing technologies to provide accurate real-time water quality measurements [161].

Microwave RS are categorized as active, also known as non-optical sensors, and passive sensors also called optical sensors. Optical sensors depend on the energy of the sun, unlike non-optical sensors which produce their energy. Although most studies have measured WQPs using optical RS, there is an opportunity to measure these parameters from the microwave region of the electromagnetic spectrum [158,159,162,163]. Passive microwave sensors detect the emitted energy within their field of view. Active microwave sensors are those sensors that provide their source of radiation to illuminate their target.

Optical RS sensors are mainly passive sensors that make use of the sun's energy. The USGS's Landsat, NASA's MODIS, the ESA's Sentinel-2, and the Medium Resolution Imaging Spectrometer (MERIS) among many others are some optical remote sensors that have been used by several scientists, including water researchers for monitoring and managing water resources [2,160,164,165]. Other known sensors used in studies include the Oceanic and Atmospheric Administration (NOAA) Advanced Very High-Resolution Radiometer (AVHRR) and the OrbView-2 Sea-viewing Wide Field-of-view Sensor (SeaWiFS) sensors [166].

Passive sensors can be either airborne or spaceborne sensors based on the platforms launched. Images from these sensors can be multispectral or hyperspectral, based on spectral and spatial resolutions. Multispectral systems collect data in 3–10 spectral bands in a single observation from the visible and the near-infrared range of the electromagnetic spectrum. The spectral bands of multispectral bands range from 0.4–0.7 μm for red–green–blue, and infrared wavelengths within the range of 0.7–10 μm, or more for near, middle, and far infrared [36,124,167]. The use of multispectral images is, however, restrictive because the spectral resolution of the images influences the quality and quantity of the information they can provide [168]. Hyperspectral RS applications offer an effective mechanism for frequent, synoptic water quality monitoring over a large spatial extent [169]. Hyperspectral sensors collect 200 or more bands enabling the construction of a continuous reflectance spectrum for all the pixels in the scene using cameras categorized as snapshot, pushbroom, or whiskbroom. The snapshot camera captures the whole image at one time. The pushbroom captures one line of the picture while the whiskbroom captures one point of the picture [2,170]. Multispectral and hyperspectral images have been used for the direct or indirect measurement of several WQPs including TSS and TDS or salinity [36,124,167]. Spaceborne sensors are those carried by satellites or spacecraft to areas outside the Earth's atmosphere. Examples of spaceborne sensors include Landsat satellite, Advanced Spaceborne Thermal Emission and Reflection Radiation (ASTER), Moderate Resolution Imaging Spectroradiometer (MODIS) Sensor, GeoEye, and IKONOS among others. Airborne sensors are mounted on platforms flown within the Earth's atmosphere. These platforms include boats, helicopters, aircraft, or balloons. Examples of airborne sensors used for capturing images for WQP monitoring include the Airborne Visible Infrared Imaging Spectrometer (AVIRIS) manufactured by NASA Jet Propulsion Lab (Pasadena, CA, USA), the Airborne Prism Experiment (APEX) manufactured by VITO (Mol, Belgium), Hyperspectral Digital Imagery manufactured by the Naval Research Lab (Washington, DC, USA), Daedalus Multispectral Scanner (MSS) manufactured by the Daedalus Enterprise Inc (Ann Arbor, MI, USA), Compact Airborne Spectrographic Imager (CASI-1500) manufactured by ITRES Research Limited (Calgary, AB, Canada), and the Multispectral Infrared and Visible Imaging Spectrometer (MIVIS) manufactured by Daedalus Enterprise Inc., (Ann Arbor, MI, USA) [36].

Both airborne and spaceborne sensors have been used in past studies to examine a wide range of WQPs since the early 1970s [171]. Airborne sensors are hyperspectral passive sensors that measure the reflectance of solar radiation throughout the visible, near and mid-infrared, and thermal regions of the electromagnetic spectrum. Images acquired are numerous but narrower. Spaceborne are also passive sensors that cover a broader geographic area compared to the coverage of airborne sensors. Spaceborne sensors make use of the constant orbital patterns of the satellite they are launched on. Images acquired by spaceborne sensors can either be multispectral or hyperspectral. The choice of a particular sensor to be used in a study depends on spectral properties and associated strengths and limitations [167]. The category of RS technologies, sensors, and images is summarized in Figure 2 below.

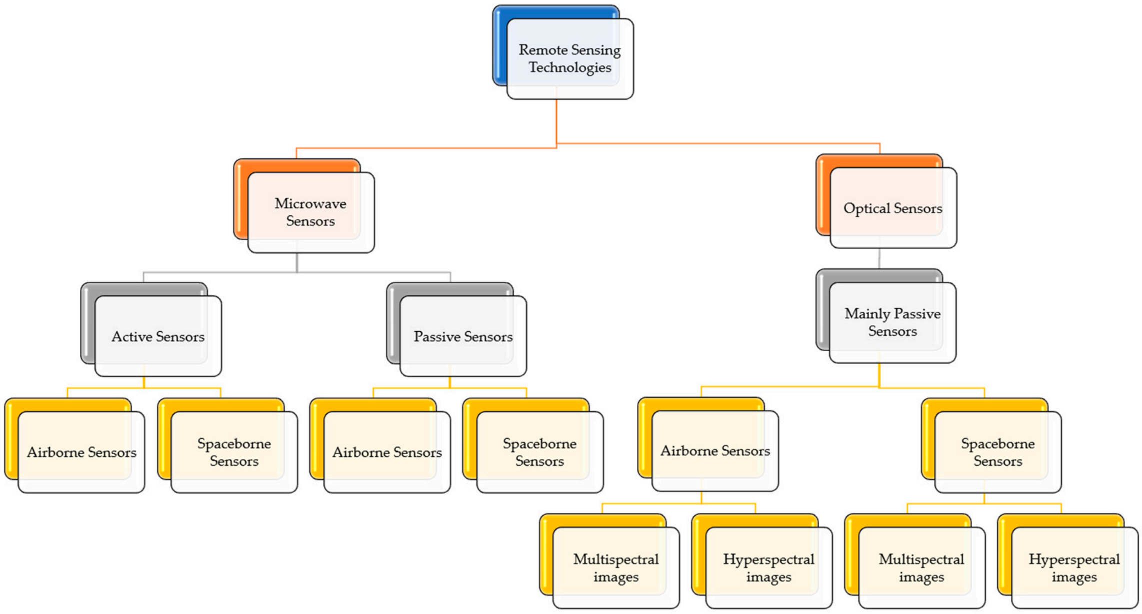

Figure 2. Summary categorization of RS technologies, sensors, and images.

A summary of some of the sensors used and proposed for capturing images for the estimation of TDS/salinity, TSSs, and their forms of occurrence are presented in Tables 2 and 3. The spatial, temporal, and spectral resolutions of the images, as well as the year of the launch of the sensor, are presented in Tables 2 and 3 [2,7,13,36,37,41,44,93,102,124,165–167,172–194].

4.2.4. RS Spectral Indices Used in Estimating TDS and TSS

RS indices combine information from two or more spectral bands. The incorporation of reflectance values from different bands through band ratios has been noted to improve the estimation of WQPs by reducing the effect of the atmosphere and further increasing the signal-to-noise ratio [41]

Several indices have been established and widely acknowledged as valuable tools in the identification of features of interest. Studies have developed indices for vegetation vigor, land use changes, and crop assessment [195]. Band ratios or indices have been used as model variables and have been found to produce good results [196]. For example, [195] used indices termed salinity indices, vegetation indices, and principal component analysis (PCA) to map and discriminate salt-affected, waterlogged areas/water bodies in Faisalabad, Pakistan. The indices used include salinity indices which are the square root of the product of the first and third bands and the normalized differential salinity index which utilizes band 3 and band 4. Additionally used were the Normalized Difference Vegetation Index (NDVI), and band ratio (Band 3/Band 4). The acquired images used were from the Linear Image Self-scanning Spectrometer (LISS-II) of the Indian RS satellite (IRS-1B). Additionally, ref. [197] found that the band ratio of 560/660 nm of radiometric data acquired with hyperspectral radiometers with a 3 nm resolution and bandwidths over the 400–700 nm range is the best ratio at $p < 0.005$ for the estimation of suspended mineral concentration for inland and coastal waters in the Vancouver Island of British Columbia, Canada.

Some of the commonly used indices include the Normalized Suspended Material Index (NSMI), the Normalized Difference Suspended Sediment Index (NDSSI), and the Band Ratio (BR) used in the analysis of suspended sediments [190,198–200]. Normalized Difference Salinity Index (NDSI), salinity indices, and TDS indices are used for the monitoring of TDS or salinity [127,189,201]. Indices utilized in the literature for monitoring TSS include the Water-Sediment Ratio Index (WSRI), the NDVI, the normalized difference water index (NDWI), and the Enhanced Green Ratio Index (EGRI) [195,200,202].

The following subsections highlight some of the indices that have been used in water quality monitoring.

Table 2. Optical Sensors used in the Estimation of TDS/Salinity and TSS with their specifications.

Satellite Sensor	Year Launched	Spatial Res. (m)	Temporal Res. (Days)	Spectral Resolution		Parameter Measured
				Number of Bands	Wavelength Range (μm)	
Sentinel-2 A/B MSI	2015	10–60	5	12	0.44–2.19	TSS, TSM, TDS
SPOT 6	2012	1.5–6.0	26	5	0.45–0.89	TSS, TSM
Landsat-4, 5 TM	1982	30–120	16	7	0.50–2.35	TSS, SSC, TSM, TDS, Salinity
Landsat-7 ETM+	1993	15–60	16	8	0.45–0.90	TSS, SM, SSC
Landsat-8 OLI/TIRS	2013	15–100	16	11	0.43–12.51	TSS, TSM, TDS, Salinity
Landsat-9 OLI-2/TIRS	2021	15–100	16	11	0.43–12.51	TSM
RapidEye	2008	5	5.5	5	0.44–0.85	TSS, SSC
Geostationary Ocean Color Imager (GOCI)	2010	500	1	8	0.41–0.87	SS, Salinity
ALOS AVNIR-2	2006	2.5–10	2	5	0.42–0.89	TSS
MERIS	2002	300–1200	1	15	0.39–1.04	TSM, TSS,
Terra ASTER	1999	15–90	16	14	0.52–11.65	TSS, TDS, Salinity
Terra MODIS	1999	250–1000	1–2	36	0.41–14.5	TSM, TSS
Aqua MODIS	2002	250–1000	1–2	36	0.41–14.5	TSM, TSS
Visible Infrared Imaging Radiometer Suite (VIIRS)	2011	375–750	0.5	22	0.50–12.01	TSS
Hyperspectral Imager for the Coastal Ocean (HICOTM)	2009	100	10	128	0.35–1.08	SPM
Earth-Observing One satellite (EO-1) Hyperion	2000	30	16	242	0.35–2.57	SM
EO-1 ALI	2000	10–30	16	10	0.43–2.35	TSS, SSC
NOAA AVHRR	1978	1000	1	5	0.60–1.20	TSS
OrbView-2 SeaWiFS	1997	1130	16	8	0.41–0.87	SS

Table 3. Microwave Sensors used in the Estimation of TDS/Salinity and TSS with their specifications.

Satellite Sensor	Year Launched/ Deployed	Spatial Res. (km)	Temporal Res. (Days)	Spectral Resolution		Parameter Measured
				No. of Bands	Wavelength Range (μm)	
NIMBUS-7 Scanning Multichannel Microwave Radiometer (SMMR)	1978	2.7–8.5	4	5	0.008–0.045	SS, Salinity
European Remote Sensing (ERS-2) SAR	1995	≤0.03	35	1	0.057	SSC
Soil Moisture and Ocean Salinity (SMOS) MIRAS	2009	3.5–50	3	1	0.212	Salinity
Scientific Application Satellite-D (SAC-D) Aquarius	2011	100	7	1	0.212	Salinity
(Airborne) Electronically Scanning Thinned-Array (ESTAR)	1990	100	-	-	0.212	Salinity
(Airborne) Scanning Low-Frequency Microwave Radiometer (SLFMR)	1999	0.5–1	-	-	0.212	Salinity
(Airborne) Salinity, Temperature, and Roughness Remote Scanner (STARRS)	2001	1	-	-	Up to 0.212	Salinity
(Airborne) Passive Active L- and S-band Sensor	1999	0.350–1	-	-	0.212	Salinity
(Airborne) Two-Dimensional Electronically Scanning Thinned-Array Radiometer	2003	0.800	-	-	0.212	Salinity
NASA Aquarius and Soil Moisture Active Passive mission (SMAP) (L-band)	2015	~40	2–3	-	0.214	Salinity

TDS and Salinity Indices

Multiple spectral salinity indices have been established in various studies. Highly reflective spectral packages are used in understanding the relationship between WQPs and spectral bands. Three water body reflectances exist for assessing WQPs using band reflectance. These are surface reflectance, bottom reflectance, and volume reflectance. To demonstrate the properties of water, a spectral range with higher reflectance is adopted. Several salinity indices which are combinations of bands in the visible and NIR range of the electromagnetic spectrum have been reported in the literature [78,189,203,204]. Clear water (i.e., water with a depth greater than 2 m) likely exhibits low reflectance in a visible range of the electromagnetic spectrum (i.e., blue, red, and green bands) There is a characteristic trend of reduction in the spectral signature value of water reflectance with increasing wavelength in the visible (band 2) and NIR infrared band [189,205]. Spectral indices used in the literature are presented in Table 4 where R = red band; B = blue band; G = green band; NIR = near-infrared band; R1 = Red_edge1 band; SWIR1 = Shortwave Infrared 1 band, SWIR2 = Shortwave Infrared 2 band, and C = Coastal band. Additionally, B1, B2, B3, B4 stand for bands 1, 2, 3, 4, and so on [54,73,168,189,206]. The wavelengths for each band for the Landsat and Sentinel platforms are provided as Appendices A and B. Landsat 8 OLI, 7 ETM+, and 5 TM are presented in Appendix A (Tables A1–A3) while Sentinel-2 MSI is presented in Appendix B (Table A4) [149,189,207–211].

Table 4. RS Indices used in estimating TDS and Salinity concentrations.

Index	Image/Data	Equation	Metrics	Study Area (Country/Region)	References
Salinity Index 1	Landsat 8 OLI	$\sqrt{R * B}$	$R^2 = 0.72$	Colorado River (USA)	[127]
			$R^2 \geq 0.72$	Shatt al-Arab River (Iraq)	[189]
Salinity Index 2	Landsat 8 OLI	$\sqrt{G * B}$	$R^2 = 0.73$	Colorado River (USA)	[127]
			$R^2 > 0.79$	Shatt al-Arab River (Iraq)	[189]
Salinity Index 3	Landsat 8 OLI	$\sqrt{R^2 + G^2}$	$R^2 = 0.72$	Colorado River (USA)	[127]
Salinity Index 4	Landsat 8 OLI	$\sqrt{R^2 + G^2 + NIR^2}$	$R^2 = 0.70$	Colorado River (USA)	[127]
Salinity Index 5	Landsat 8 OLI	$G * R$	$R^2 = 0.73$	Colorado River (USA)	[127]
			$R^2 \geq 0.44$	Shatt al-Arab River (Iraq)	[189]
	Landsat 5 TM		$R^2 > 0.65$	Coastal surface water (Bangladesh)	[212]
	Landsat 8 OLI	$G * R$	$R^2 > 0.49$		
Salinity Index 6	Landsat 8 OLI	$\sqrt{G^2 * NIR^2}$	$R^2 = 0.71$	Colorado River (USA)	[127]
Salinity Index 7	Landsat 5 TM		$R^2 > 0.06$	Coastal surface water (Bangladesh)	[212]
	Landsat 8 OLI	$\frac{B}{G}$	$R^2 > 0.46$		
-	ASTER	$\frac{B5}{B3} * B7$	$R^2 > 0.57$	Qaroun Lake (Egypt)	[206]
NDSI	Landsat 8 OLI	$\frac{R-NIR}{R+NIR}$	$R^2 > 0.51$	Mekong Delta (Vietnam)	[213]
TDS 1	Sentinel-2 MSI	$G + R + R1$	$r \geq 0.79$	Guartinaja and Momil wetlands (Colombia)	[54]
TDS 2		$\frac{G+R-R1}{G+R+R1}$	$r \geq 0.00$		
TDS 3		$\frac{R1-B}{R1+B}$	$r \geq 0.52$		
TDS 4		$R1 + R - B$	$r \geq 0.79$		
TDS 5		$R1 + R$	$r \geq 0.79$		
TDS 6		$\frac{R+R1}{SWIR1+SWIR2}$	$r \geq 0.00$		
TDS 7		$\frac{R*R1}{SWIR2}$	$r \geq 0.00$		

R = red band; *B* = blue band; *G* = green band; *NIR* = near-infrared band; *R1* = Red_edge1 band; *SWIR1* = Shortwave Infrared 1 band, and *SWIR2* = Shortwave Infrared 2 band. *B1*, *B2*, *B3*, *B4* stand for bands 1, 2, 3, 4, and so on.

TSS and Sediment Indices

Indices used for the estimation of TSS indices include the Normalized Suspended Material Index (NSMI), the Normalized Difference Suspended Sediment Index (NDSSI), the Band Ratio (BR), and other established indices.

Values of NSMI and NDSSI range from −1 to +1. Lower values of NSMI correspond to clearer water. When the blue band has a higher value than the sum of the red and green bands, the equation gives a negative value, indicating the presence of clearer water. Higher values correspond to water with more SM. Sediment also increases the reflectance of the green range of the spectrum [198]. Higher values of NDSSI, however, indicate the presence of clearer water and lower values indicate the presence of more turbid water or land. BR ranges from 0 to infinity. The highest value indicates the presence of more suspended sediments. A study found NSMI to have a better performance in estimating TSS compared to NDSSI because the wavelength of visible bands as associated with NSMI have greater penetrating power in the water surface compared with infrared bands [199]. Another study by [198] utilized NSMI to identify SM by using Landsat 7 Enhanced Thematic Mapper (ETM+) satellite data on the coast of Cabo Rojo in Puerto Rico. Results obtained from the NSMI were compared to other indices, such as the NDSSI and BR, and found similar patterns and indications of validity of the results. Although the NSMI was found to be successful in distinguishing between clear water and suspended material in a study performed in Cabo Rojo in Puerto Rico, it was unable to identify suspended matter in shallow areas such as coral reefs and swamps. Spectral indices used in the literature for the study of TSS and its related forms are presented in Table 5.

Table 5. RS indices used in estimating TSS and its Forms.

Index	Image/Data	Equation	Metrics	Study Area (Country/Region)	References
NSMI	Landsat 7 ETM+	$\frac{R+G-B}{R+G+B}$	$R^2 \geq 0.96$	Lake Mead (USA)	[190]
			-	Cabo Rojo (Puerto Rico)	[198]
			$R^2 > 0.51$	Barito Delta (Indonesia)	[199]
	Landsat 8 OLI		$R^2 > 0.70$	Dams (South Africa)	[200]
NDSSI	Landsat 7 ETM+	$\frac{B-NIR}{B+NIR}$	-	Lake Mead (USA)	[190]
			-	Cabo Rojo (Puerto Rico)	[198]
			$R^2 = 0.01$	Barito Delta (Indonesia)	[199]
			$R^2 > 0.66$	Mississippi River Lake Pontchartrain (USA)	[214]
BR	Landsat 7 ETM+	$\frac{G}{B}$	-	Lake Mead (USA)	[190]
				Cabo Rojo (Puerto Rico)	[198]
			$R^2 = 0.05$	Barito Delta (Indonesia)	[199]
WSRI	Landsat 8 OLI	$1-\left(\frac{SWIR-B}{R}\right)$	$R^2 > 0.70$	Dams (South Africa)	[200]
EGRI	Landsat 8 OLI	$\frac{G}{C+B}$	$R^2 > 0.70$	Dams (South Africa)	[200]
NDVI	Landsat 8 OLI	$\frac{NIR-R}{NIR+R}$	$R^2 > 0.70$	Dams (South Africa)	[200]

R = red band; *B* = blue band; *G* = green band; *NIR* = near-infrared band; *SWIR1* = Shortwave Infrared 1 band, *SWIR2* = Shortwave Infrared 2 band, and *C* = Coastal band.

4.2.5. Summary of Studies on TDS and TSS Estimation with RS Applications

RS applications have also been used in the analysis and estimation of TSS and TDS in water bodies. The impact of TSS concentrations on the reflectance is clear and substantial making it one of the most successful parameters to be measured using RS applications [118]. Satellite and airborne imagery have become valuable tools for scientists to map, assess, and monitor the spatial distribution of suspended sediments. RS is used in combination with in situ measurements to assess and monitor the distribution of WQPs such as TSM [215]. RS spectral indices have been used in determining suspended sediment distributions.

Empirical regression algorithms have been used in the determination of salinity or TDS using reflectance data obtained from spaceborne optical sensors such as Landsat 5 TM, Landsat 7 ETM+, Landsat 8 OLI, and other satellite images [44,156,216]. Salt or ion accumulations affect the reflectance of electromagnetic radiation as it interacts with the water.

Microwave-based RS sensors used for monitoring salinity include the STARRS, SLFMR, and Nimbus-7 SMMR. The STARRS is an enhanced version of the Scanning Low-Frequency Microwave Radiometer. The STARRS sensor accepts input data and improves salinity retrieval accuracy [217]. Microwave sensors have been found to provide accurate measurements of ocean salinity and temperature because the emission measured by the microwave systems is sensitive to the dielectric constant or the permittivity, which is dependent on the water salinity and temperature [132]. The sea surface temperature and salinity are important in determining the density of seawater which is a critical indicator driving the currents of the ocean. Ocean circulation is a critical phenomenon to analyze global water balance, evaporation rates, and productivity forecast models [36]. Although the RS sensors are effective in the monitoring of water quality of ocean waters, their usage in fresh waters such as rivers and lakes may be limited due to very large pixel sizes (coarse spatial resolution) varying to kilometers [132], which are larger than many freshwater systems.

Studies have reported satisfactory performance using microwave sensors for the estimation of salinity/TDS and TSS in ocean waters. Examples include the study by [218] where ship-borne microwave radiometer data were used to develop improved sea surface microwave emission models or algorithms for the retrieval of sea surface salinity. The authors found root mean square error (RMSE) or differences between the in situ and retrieved sea surface salinity of around 0.4 Practical Salinity Units (PSU) which indicates good model performance. Another study by [219] measured the variability in sea surface salinity by the Aquarius and SMOS satellite missions using an assimilation scheme as described by researchers in [220] and obtained a RMSE of <0.1 PSU between derived and field surface salinity in most of the ocean with a global median value of 0.05 PSU. Additionally, the NASA Aquarius, in situ field, and Hybrid Coordinate Ocean Model (HYCOM) products were used to assess sea surface salinity in a study by [221]. The study found RMSE for Aquarius Level-2 and Level-3 data to be 0.17 PSU and 0.13 PSU, respectively, using triple point analysis.

Researchers in [55] used microwave SAR and thermal images and an inversion technique applied to the models of scattering to estimate WQPs including TDS and salinity in high-precision SAR and thermal images. Analysis of the results pointed to the potential of identifying WQPs with superior precision using microwave sensors. Researchers in [222] used an airborne scanning low-frequency microwave radiometer and in situ bio-optical variables to estimate WQPs including SS for Florida Bay located in the southern tip of the state of Florida, USA using empirical relationships or algorithms. The study found the average salinity for the outer and central bay stations to be 31.2 PSU and 23.6 PSU, respectively. The study also found that the concentration and variability of TSS were greater in the outer bay as compared to the central bay stations. Average TSS concentrations of 14.4 mg/L and 2.8 mg/L were recorded, respectively, for the outer and central bay stations. Inorganic composition counted for 70% and 15% of the TSS loads, respectively, for the outer and central bay stations. Results from the study demonstrate the significance of salinity measurement in delineating bio-optical regimes useful for the development of regional ocean color RS techniques for coastal waters.

TSS estimations have also been successfully carried out in rivers, reservoirs, and estuaries using empirical regression algorithms or analyses. These analyses are performed with in situ measurements and reflectance data from airborne RS and spaceborne optical sensors, including Landsat (4 and 5) TMs, (7) ETM+, (8) OLI, and other sensors. Airborne RS produces more accurate results in TSS estimations in rivers and reservoirs, owing to less atmospheric interference, fewer temporal restraints, and adaptable spatial resolutions [44,119,156,214,223,224].

The following paragraphs summarize some of the work that has been performed on the estimation of TSS and TDS using RS applications.

Researchers in [192] applied empirical neural networks in the estimation of WQPs, including SSC, in the Gulf of Finland using combined optical (Landsat 5 TM) and microwave data (ERS-2 SAR). Results indicated that the neural network was adequate in describing the nonlinear transfer function between the optical and microwave sensors and the water surface parameters as compared to the regression analysis. The optical bands produced an R^2 of 54% and 89% for regression and neural network analyses, respectively. The reported performance when optical and microwave bands were fused was slightly higher (55% and 91%, respectively, for regression and neural network analyses). Analysis of the results also showed a difference in RMSE between the optical and the optical/microwave fused bands of 0.01 mg/L and 0.007 mg/L, respectively, for the regression and neural network analyses. A similar study by [179] compared the results of MODIS-Landsat fusion to single-band algorithms for TSS estimations. The algorithms employed in this study included the Aqua-MODIS-based spectral model, Landsat and synthetic Landsat images, and copula integrated fusion model. The study found the fusion model to have a better performance in the TSS estimations in dynamic river systems compared to the single-band MODIS model due to the finer spatial resolutions of the fusion model. The reported R^2 for the MODIS-based model was 65–77% while that of the Landsat-MODIS fused model increased up to 85–89%.

Researchers in [225] explored the possibility of using MODIS 250 m and 500 m resolution bands at 469 nm, 555 nm, and 645 nm for the monitoring of water quality indicators including TSS in Tampa Bay, FL, USA. Tampa Bay is the largest open-water estuary in the State of Florida, USA with an approximate area of 910 km^2. Field sampling conducted shows that Tampa Bay has Case-II waters (waters in which the parameters studied do not co-vary) with a salinity range of 24–32 PSU and TSS of 2 to 11 mg/L. The authors established a regression model for the total radiance measured by the MODIS and the WQPs, which were subsequently used to develop a synoptic map of suspended sediments. The authors found a significant R^2 of 90% for a sample size of 31 between TSS and the spectral RS reflectance value of the 645 nm band of the MODIS image using empirical regression.

Researchers in [226] also used the 250 m resolution to map concentrations of TSM in coastal waters located in the Northern Gulf of Mexico. The study established a linear relationship between in situ TSM measurements and band 1 of the MODIS Terra 250 m image with 620–670 nm wavelength and found an R^2 of 89% for a sample size of 52.

Researchers in [227] used reflectance band ratios to estimate suspended and dissolved matter concentration in the Tamar estuary located in the southwest UK using in situ hyperspectral remote-sensing reflectance measurements. The study obtained a strong R^2 of 96% between the NIR (wavelength of 850 nm) to visible reflectance (wavelength of 550 nm) (visible/NIR) ratio of the compact airborne spectrographic imager (CASI) and the TSM concentrations.

Researchers in [228] compared several ML algorithms including ANN, SVR, random forest, and cubist regression for the retrieval of WQPs including concentrations of suspended solids in the coastal waters of Hong Kong using in situ reflectance (CROPSCAN Multispectral Radiometer (MSR)) and satellite data (Landsat 5 TM, Landsat 7 ETM+, and Landsat 8 OLI). The authors found the ANN to be the model with the highest accuracy for estimating TSS with R^2 of 92% and 93% for the satellite data and in situ reflectance data, respectively.

Researchers in [229] used ANN to investigate and assess WQPs. The study establishes a relationship between the reflectance from Landsat 5 TM data for different bands (i.e., band 1 to band 7) and WQPs including suspended sediments for the Beaver Reservoir located in Arkansas, USA. The Beaver Reservoir is the main source of drinking water for more than 300,000 people in the northwestern part of the state of Arkansas with a surface area of 103 km^2 and with a depth ranging from 18 to 60 m. The study first linearly regressed the combination of bands termed as indices and found moderate predictions for estimations for most of the indices utilizing the first three bands (R values of 0.21 to −0.69). Further analyses were performed by feeding the bands and indices values into an ANN model for the estimation of WQPs. The ANN model produced an 81.6% to 98.2% efficiency for the estimation of suspended sediments with the highest efficiency coming from an ANN model using bands 1 to 4. This model was trained at an efficiency of 98%.

Researchers in [214] developed an RS-based index from Landsat 7 ETM+ to estimate and map SSC in a river and lake environment in the USA. The study explored the possibility of using RS Landsat images to estimate coefficients that could further predict SSC in periods where in situ field measurements become impossible due to extreme events using empirical relationships or algorithms. The authors found the model with power relations yielding R^2 of 73.8% to show potential for the estimation of SSC for the Mississippi River and

Lake Pontchartrain located in Louisiana, USA for the Bonnet Carre Spillway opening event and before and after Hurricane Katrina. Results were compared with simulations from CCHE2D: a numerical model developed by the National Center for Computational Hydroscience and Engineering (NCCHE) for unsteady turbulent flow simulation. Results were in good agreement quantitatively and qualitatively [214].

Researchers in [230] retrieved the TSM and chlorophyll-a concentration using the Indian Remote-Sensing Satellite (IRS-P6). Analysis of the water quality data and satellite-received radiances signals using empirical regression and ANN models or algorithms. Results showed that the empirical models produced an R^2 of 94% for TSM. The performance accuracy improved significantly with the ANN model with R^2 of 98% for the TSM concentration. RMSEs produced were 15% and 7.5%, respectively, for the empirical and ANN models. Researchers in [102] developed an RS-based early warning system for monitoring TSS concentration in Lake Mead located in a water-scarce area in the US. This study applies integrated data fusion and mining (IDFM) capabilities to develop an almost real-time monitoring system for daily predictions of TSS concentrations. The study further applies a model called the nonlinear autoregressive neural network input (NARXNET) model for the time series of forecasting of TSS concentrations using the IDEFM techniques. This forecast shows no direct influence of forest fire events in accelerating the rise of TSS concentrations. The study, however, found a probable impact of drought on increasing TSS concentrations in the Overton and Colorado River Arms of Lake Mead.

Researchers in [231] applied GIS and RS techniques for the monitoring of several WQPs including TDS and TSS using empirical linear regression in Lake Al-Habbaniyah, Iraq. The authors compared remotely sensed results from Landsat 8 OLI to in situ measurements and reported a variation of 147–1520 mg/L and 68–3200, respectively, for TDS and TSS. Results indicate a probable significant correlation between bands 2 and 3 with TDS for autumn and summer. TSS has a probable strong correlation with band 2 during the autumn. The study estimates the highest r in TDS (0.94 at p = 0.016) and the highest r (0.73 at p = 0.158) for band 2 reflectance.

Researchers in [166] performed a study to quantify surface river SS along a river-dominated coastline in Louisiana, USA using statistical models including correlation, linear and nonlinear algorithms or techniques. The study used data acquired by the NOAA AVHRR and the Orbview-2 SeaWiFS ocean color sensors. Field measurement samples used in the study were obtained using a helicopter, small boat, and automatic water sampler within a few hours of the satellite overpasses. The study used satellite and field measurements to develop statistical models for the estimation of near-SS and surface-suspended sediments. Analysis shows that the NOAA AVHRR Channel 1 (580–680 nm), Channel 2 (725–1100 nm), and SeaWiFS Channel 6 (660–680 nm) with a cubic, linear, and power model, respectively, were the best models for surface SSC predictions. The SeaWiFS Channel 5 (545–565 nm) was found to perform poorly. The authors attribute the inferior performance to reasons including the type of atmospheric correction technique applied, the shallow depth of the water samples collected, and the absorption effects from non-sediment water constituents.

Researchers in [169] developed an empirical algorithm using hyperspectral RS. The water irradiance reflectance spectra were acquired with dual Ocean Optic 2000 spectroradiometers (USB2000) with a sample size of 53 and about 2000 bands and a sampling interval and spectral resolution of approximately 0.3 nm and 1.5 nm, respectively. The study was carried out on the Patuxent River, a large tributary of Chesapeake Bay in the USA with a 2427 sq. km watershed area. The study developed empirical models using water reflectance for the retrieval of WQPs including TSS and found that the ratio of green to blue spectral bands was the best predictor of TSS (R^2 of 75% was established).

Researchers in [180] used a robust algorithm for the estimation of TSS in inland and nearshore coastal waters using a Statistical, inherent Optical property (IOP)-based, and muLti-conditional Inversion proceDure (SOLID) approach developed from semi-analytical, ML, and empirical models. To demonstrate the performance of the SOLID model, the model was implemented for images acquired by MultiSpectral Imager aboard Sentinel-2A/B over the Chesapeake Bay, San-Francisco-Bay-Delta Estuary, Lake Okeechobee, and Lake Taihu. It was established that the SOLID approach has the potential for producing TSS products in global coastal and inland waters. To obtain consistent, multi-mission TSS products, the model performance was extended and evaluated for other satellite missions including the OLCI, Landsat 8 OLI, MODIS, and VIIRS. Results obtained from statistical analysis showed the SOLID model improved retrieval performances offered by five widely used TSS retrieval methods for global and all water types. Comparing results to other models used in other studies shows improvement in the SOLID model to other models. For example for global waters, the statistical performance of the SOLID model had a median absolute percentage error (MAPE) of 49%, root means squared logarithmic error of 0.32, the mean absolute error (MAE) computed in log-space of 1.81, and log-transformed residuals (bias) of 1.09 compared with MAPE, MAE, RMSE, Bias of 58.82%, 2.56, 0.53, and 0.50, respectively, obtained by [226], MAPE, MAE, RMSE, Bias of 59.74%, 2.31, 0.46, and 1.26, respectively, obtained by [215,226], MAPE, MAE, RMSE, Bias of 57.71%, 2.17, 0.41, and 0.70, respectively, obtained by Petus et al. (2010), MAPE, MAE, RMSE, Bias of 68.38%, 2.28, 0.46, and 1.60, respectively, obtained by [148] and MAPE, MAE, RMSE, Bias of 52.73%, 1.92, 0.35, and 1.27, respectively, obtained by [138].

Researchers in [232] evaluated the radiometric and spatial performance of Chinese high-resolution GF-1 Wide Field Imager (WFI) data for monitoring SPM using inversion and regression models. Results obtained from GF-1 data were compared to outputs from the Landsat 8 OLI and MODIS (250 and 500 m) resolution bands. High consistency in spatial distribution and concentration of SPM maps was seen between the GF-1 and Landsat 8 OLI data. More than 75% of the spatial variations in turbidity were resolved by the GF-1 while only 40% were resolved by the MODIS band with 250 m resolution.

Researchers [233] used the NDVI to assess how catchment condition varies within and across river catchments in Zimbabwe. The study used a non-linear regression to check if the NDVI is significantly related to the levels of TSS. Results from the analysis showed a consistent negative curvilinear relationship between the NDVI derived from the Landsat 8 OLI and TSS measured across the catchments under study. A total of 98% of the variations in TSS are explained by the NDVI in the drier catchments with 64% of the variations in TSS explained by the NDVI in the wetter catchments at the 0.05 significance level. The results showed a consistent negative curvilinear relationship between Landsat 8 OLI-derived NDVI and TSS measured across the catchments under study.

Researchers in [234] reported a linear relationship between reflectance and TSS at concentrations from 1 to 500 mg/L for a study conducted at the Didipio catchment located in the northern territory of the Philippines with a surface area of 39.25 km^2 using remote sensing images and empirical regression models. The catchment area is made of seven rivers (i.e., Dupit, Alimit, Surong, Camgat, Camgat-Surong, Didipio, and Dinauyan Rivers). The authors found that reflectance increases at a lower and variable rate in the concentration ranges of 500 to 3580 mg/L. This study used three different satellite sensors namely, 5 m resolution RapidEye, 2 m resolution Pleiades-1A, and 6 m SPOT 6 images. The study finds consistency in the model developed with the red band data for the various images and reports an R^2 value of 65% for all three sensors.

Researchers in [235] used Landsat 7 ETM+ and Landsat 8 OLI sensors to monitor WQPs, including TSM in a nutrient-rich (hypereutrophic) Qaraoun Reservoir in Lebanon. The study area has a surface area and median depth varying from 4 to 10 sq. km and 10 to 20 m, respectively. The reservoir has a maximum depth of 45 m. The study develops empirical algorithms to quantify the parameters of interest. In general, ETM+ sensors have improved performance compared to OLI sensors for this study. R^2 was 81% for the ETM+ models and 58% for the OLI-based models. Results confirmed the effectiveness of using Landsat-based models to quantify WQPs in a semi-arid hypereutrophic reservoir, which presents the opportunity to improve the spatiotemporal coverage of data cost-effectively.

Researchers in [200] used Landsat 8 OLI RS spectral indices and empirical regression models for mapping SS in various dam impoundments located in South Africa. These dams include Spring Grove Dam, Midmar Dam, Nagle Dam, Albert Falls Dam, and the Inanda Dam. The indices this study considered were NSMI, WSRI, NDVI, and EGRI. The NSMI was the most effective index among the studied indices for the mapping of SS in the study area. Other spectral indices in the visible to shortwave infrared also produce reasonable estimations (R^2 of 70% at $p < 0.05$). The NSMI showed greater accuracy for the mapping of WQPs, as opposed to two-band spectral indices. The authors recommend comparing these results to other indices derived from high-resolution images such as Sentinel-2 and Ziyuan-3.

Researchers in [236] retrieved and mapped chlorophyll-a and TSS using Sentinel-2A images and Cubist ML models. Water samples used in the study were collected from water reservoirs within the southern part of the Czech Republic in Central Europe. The authors reported an R^2 of 80% for the accurate prediction of TSS. The study found dramatic temporal changes in the values of TSS in fishponds compared to sand lakes. Differences in the management practices in these water bodies were linked to the dramatic changes in TSS values over time.

Researchers in [208] assessed the impact of LULC on groundwater quantity and quality in Ajman City and its adjoining area located in the United Arab Emirates (UAE). The study correlated a Spectral Angle Mapper (SAM) and NDVI of Landsat 7 ETM+ and Landsat 8 OLI with WQPs including TDS. Analysis of the spatial extents revealed a sharp depletion in the quality and quantity of groundwater related to an increase in LULC. The mean TDS reported was about 24,210.5 mg/L with a groundwater depth of 14.8 m for 15 years.

Researchers in [157] used the NDWI indices of Landsat 8 OLI images as an effective tool to determine surface WQPs including TDS and TSS concentrations using step-wise regression-based models for the Bijayapur River flowing through Pokhara in Nepal. Reported TDS concentration ranges from about 244 to 1145 mg/L while TSS concentrations range from 0 to 750 mg/L.

Researchers in [237] used Landsat 8 OLI and forward regression analysis to develop models for the estimation of WQPs including TDS and TSS in the Tubay River located in the Philippines. The study found an R^2 of 96.8% for TDS and $\geq$24.4% for the regression models.

Another study by [238] developed an empirical regression algorithm to assess WQPs, such as TDS, EC, and water temperature, in the Tigris and Euphrates rivers in Iraq by using Landsat 5 TM. The stations used for the water quality monitoring were situated in Diyala and Baghad cities along the 120 km stretch of the Tigris River, and Ramadi and Karbala cities along the 277 km stretch of the Euphrates River. The model developed showed a significant correlation between models and WQPs with $R^2 > 0.83$. The measured and predicted TDS ranged from 350 to 550 mg/L.

Researchers in [203] also established a correlation between water extraction indices of Landsat 8 OLI and WQPs including TDS and TSS for the Tigris River for different type periods and found correlation of -0.808 between TDS and WRI and r of 0.651 for TSS and AWEI for the samples collected on 11 May 2017 in five stations in a stream of 15–20 m width. Field-measured TDS concentrations ranged from 450 to 646 mg/L while TSS ranged from 16 to 54 mg/L for the five stations on the said date.

Researchers in [239] correlated values of different Landsat 8 OLI sensor bands with the measured TDS and established a regression model for the estimation of TDS. The authors investigated the use of Digital Numbers (DN) of atmospherically corrected Landsat 8 OLI images in estimating TSS and TDS in Mosul Dam Lake located in Iraq using linear corrections between the reflectance values and the in situ field measurements. Bands 1, 5, and 6 were found to correlate to TSS for summer, spring, and autumn, while bands 3, 6, and 7 significantly correlated to TDS for autumn, summer, and spring. The highest R^2 values of 31% and 41% were obtained for TSS and TDS, respectively, in July.

Researchers in [26] utilized several ML models for estimating WQPs including TDS in Lake Tana located in the Tropical Highlands of Ethiopia, using Landsat 8 OLI images.

The authors found the random forest regressors to be the best performing model for the estimation of TDS, which performed best for the TDS R^2, NSE, MARE, and RMSE of 79%, 0.80, 0.082, and 12.30 mg/L, respectively, for features such as the outcomes of (B4 + B3)/2, (B4 + B2)/2, (B3 + B2)/2, and (B2 + B3 + B4)/3.

Researchers in [240] assessed the water quality of River Beas in India using Landsat 5 TM imagery through multivariate and RS applications for pre- and post-monsoon seasons. They established that TDS correlates positively to the green band and negatively to the red band, using multiple linear regression and β-regression analysis. There was also a highly significant correlation between the predicted and observed values from an ANN for the parameters measured at $p < 0.001$. The study, however, did not report the R^2 values obtained.

Researchers in [189] used band reflectance and a combination of bands termed salinity indices in estimating TDS in the Shatt al-Arab River in Iraq using simple linear regression. Measured TDS were within the range of 800 to over 37,000 mg/L. Reported R values in this study were within a range of 0.70 to 0.97 with R^2 being in the range of 56 to 94% between in situ measurements and spectral data of Salinity Index 2. Salinity Index 2 is the square root of the product of green and blue bands of the Landsat 8 OLI.

Researchers in [54] also used RS spectral indices to estimate TDS in the freshwater Guartinaja and Momil wetlands located in the Wetland Complex of Bajo Sinú, Northern Colombia. The authors utilized Sentinel-2 images in establishing empirical regression models for TDS estimations. Field measured TDS concentration ranged from about 154–218 mg/L. The study used ten spectral bands of the Sentinel-2 image and 11 indices which have been used in literature for the estimation of water, vegetation, or soils, and 2 indices developed by the authors. The model performed with high accuracy with a recorded normalized RMSE of <10%.

Researchers in [241] retrieved TDS concentrations from WQPs such as TSS obtained from drinking, ground, and surface waters for a study performed in a mining community of Tarkwa located in Ghana using models such as Gaussian process regression, principal component regression, and backpropagation neural network models. The findings reveal average R^2, RMSE, and MAE, of 98.7%, 4.090 mg/L, and 7.910 mg/L, respectively.

Additionally, researchers in [242] also used Sentinel-2 and Landsat 8 OLI coupled with the ANN model to retrieve and map the spatiotemporal variability of salinity in Lake Urmia in Iran. The results of the ANN model were compared with outputs from the Adaptive Network-based Fuzzy Inference System and the multiple linear regression models. The findings show that the ANN was superior in the accurate retrieval of the salinity concentration from the surface water reflectance with an obtained R^2 of 94%.

A summary of studies carried out to retrieve optically active TSS and optically inactive TDS using RS applications and statistical and machine learning models, or algorithms and the degree of accuracy established are presented in Tables 6 and 7.

4.2.6. Strengths and Drawbacks of RS Methods for Measuring TDS and TSS

The concentrations of TDS and TSS in water are some of many environmental phenomena that may be efficiently monitored using cutting-edge, modern, and advanced RS techniques. The use of RS to measure and monitor TDS and TSS has produced promising results in the assessment of water quality [34,40,129,189,190,198,239]. However, some limitations and difficulties must be noted, as with any technology. These strengths and drawbacks are summarized in Table 8 [2,10,36,124].

Table 6. RS Application Models for the Retrieval and Estimation of TDS/Salinity and its Forms.

Sensor/Data	Model/Algorithms	Metrics	Study Area (Country/Region)	References
ASTER	Empirical	$R^2 > 0.50$	Qaroun Lake (Egypt)	[206]
Landsat 8 OLI	ML	$R^2 = 0.79$	Lake Tana (Ethiopia)	[26]
Landsat 8 OLI	Empirical	$R^2 > 0.00$	Coastal Surface Water (Bangladesh)	[243]
Landsat 5 TM, 8 OLI	Empirical	$R^2 \geq 0.76$	Coastal Surface Water (Bangladesh)	[212]
Landsat 8 OLI	Empirical	$R^2 \geq 0.62$	Colorado River (USA)	[127]
Landsat 8 OLI	Empirical	$R^2 \geq 0.83$	Lake Al-Habbaniyah (Iraq)	[231]
Sentinel-2 MSI	Empirical	$R^2 > 0.70$	Guartinaja, Momil wetlands (Columbia)	[54]
Landsat 8 OLI	Empirical	$R^2 > 0.84$	Gorano Dam (Pakistan)	[244]
Landsat 8 OLI, Sentinel-2 MSI, Göktürk-2	ML	$R^2 \geq 0.51$	Lake Gala (Turkey)	[245]
Landsat 8 OLI	Empirical	$R^2 > 0.55$	Shatt al-Arab River (Iraq)	[189]
Landsat 8 OLI	Empirical, ML	$R^2 \geq 0.68$	Karun River Basin (Iran)	[246]
GOCI	Empirical	PMARE = 0.75%	Southern Yellow Sea (China, North and South Korea)	[247]
Landsat 8 OLI	Empirical	$R^2 \geq 0.60$	Arabian Gulf (Middle East)	[248]
Landsat 5 TM	Empirical	$R^2 = 95$	Tigris and Euphrates Rivers (Iraq)	[238]
Ship-borne microwave radiometer	-	RMSE $\approx$ 0.4 PSU	East China Sea (China)	[218]
Landsat 8 OLI	Empirical	$R^2 > 0.96$	Tubay River (Philippines)	[237]
IRS LISS III	Empirical	$R^2 > 0.46$	Gomti River (India)	[249]
Landsat 8 OLI	Empirical	$R^2 > 0.13$	Mosul Dam Lake (Iraq)	[239]

Table 7. RS Application Models for the Retrieval and Estimation of TSS and its forms.

Sensor/Data	Model/Algorithms	Metrics	Study Area (Country/Region)	References
Unmanned Aerial Vehicle (AV) multispectral images, Landsat 8 OLI	ANN, Empirical	$R^2 > 0.60$	Lake at Unisinos University (South Brazil)	[202]
Landsat 5 TM, Landsat 8 OLI, and Chinese GaoFen-1 (GF-1) Wide Field of View (WFV)	Wen, Nechad, and Novoa algorithms	$R^2 > 0.88$	Min River (China) (TSS)	[250]
Landsat 5 TM	Empirical	$R^2 > 0.23$	Reelfoot Lake, Tennessee (USA)	[119]
MERIS, OLCI	Semi-analytical	$R^2 \geq 0.25$	Lakes Kasumigaura, Suwa, Akan (Japan), Lake Taihu (China), Lac Vieux Desert, Lakes Winnebago, Poygan, Winneconne, Green Bay of Lake Michigan (North America)	[251]
Landsat 8 OLI	Empirical	$R^2 \geq 0.71$	Dam impoundments (South Africa)	[200]
Sentinel-2 MSI	Empirical	$R^2 = 0.85$	Negro River, Amazon Basin (Brazil)	[137]
Landsat 8 OLI, MODIS	-	$R^2 \geq 0.40$	Poyang Lake (China)	[232]
Landsat 5 TM	Semi-analytical model	$R^2 \geq 0.51$	Gulf of Bohai (China)	[135]
Ocean Optic 2000 spectroradiometers (USB2000)	Empirical	$R^2 = 0.75$	Chesapeake Bay (USA)	[169]
Landsat 8 OLI	Empirical	$R^2 \geq 0.87$	Lake Al-Habbaniyah (Iraq)	[231]
Landsat 7 ETM+	Empirical	$R^2 > 0.66$	Mississippi River and Lake Pontchartrain (USA)	[214]
SPOT 6	Empirical	$R^2 = 0.65$	Didipio catchment (Philippines)	[234]
MODIS	Empirical	$R^2 = 0.89$	Lake Pontchartrain, Mississippi River, Mississippi Sound (USA)	[226]
MODIS	Empirical	PMARE = 25.5%	Yangtze river (China)	[134]
Landsat 5 TM, Landsat 7 EM+, MODIS	Empirical	$R^2 \geq 0.13$	Yangtze river (China)	[252]
MODIS	Neural Network	$R^2 > 0.60$	Bohai Sea, Yellow Sea, East China Sea (China)	[253]
Landsat 9 OLI-2, Sentinel-2	Bio-Optical Model	$R^2 \geq 0.17$	Lakes Trasimeno, Maggiore, and Mantova (Italy)	[181]
MODIS, Landsat 8 OLI	Copula-based enhanced nonlinear	$R^2 \geq 0.31$	Hooghly River (India)	[179]
ALOS/AVNIR-2	Empirical	$R^2 \geq 0.71$	Monobe River (Japan), Altamaha River (USA), St. Mary's River (USA)	[183]
LISST-200x and EXO2 Multiparameter Sonde sensors	Empirical	$R^2 \geq 0.67$	Coastal regions	[254]
Landsat 7 ETM+, Landsat 8 OLI	Empirical	$R^2 \geq 0.16$	Qaraoun Reservoir (Lebanon)	[235]
Landsat 8 OLI	Empirical	$R^2 \geq 0.64$	Thirty-two sub-catchments (Zimbabwe)	[233]
Landsat 5 TM	Neural Network	$R^2 > 0.90$	Beaver Reservoir (USA)	[229]
MODIS	Empirical	$R^2 > 0.80$	Green Bay of Lake Michigan (USA)	[255]
Sentinel-2 MSI	Semi-empirical	$R^2 \geq 0.63$	Yangtze Main Stream (China)	[131]
MODIS	Empirical, ML	$R^2 > 0.27$	Chesapeake Bay (USA)	[129]
CASI	Empirical	$R^2 > 0.84$	Tamar estuary (UK)	[227]
Landsat 8 OLI	Empirical	$R^2 > 0.73$	Orinoco River (Venezuela)	[256]
OLCI				
Landsat 4,5 TM, 7 ETM+, 8 OLI	Empirical	$R^2 \geq 0.58$	Estuaries and Coasts (China)	[257]
Chinese HJ-1A/CCD	Semi-analytical	$R^2 > 0.66$	Oujiang River Estuary (China)	[258]
MODIS	Empirical	$R^2 = 0.90$	Tampa Bay (USA)	[225]
Sentinel-2A MSI	Semi-empirical, ML	$R^2 = 0.80$	Water Reservoirs (Czech Republic)	[236]
Landsat 8 OLI	AI	$R^2 > 0.93$	Saint John River (Canada and USA)	[259]
Sentinel-2 A/B MSI	Empirical	$R^2 > 0.13$	Sado Estuary (Portugal)	[93]
Landsat 8 OLI	Empirical	$R^2 > 0.10$	Mosul Dam Lake (Iraq)	[239]
IRS LISS III	Empirical	$R^2 > 0.23$	Gomti River (India)	[249]
Landsat 8 OLI, Sentinel-2 MSI, Göktürk-2	ML	$R^2 \geq 0.64$	Lake Gala (Turkey)	[245]
Landsat 8 OLI, Sentinel-2 MSI	Empirical, Semi-empirical	$R^2 \geq 0.81$	Hedi Reservoir (China)	[34]
HICO^{TM}	Semi-empirical	$R^2 = 0.85$	Northern Adriatic Sea	[260]

Table 8. Strengths and limitations of the RS applications in measuring and monitoring TDS and TSS.

Strengths	Limitations
Provides a synoptic overview of the entire water body	Accuracy may be limited
Easy access and acquisition of open source	Image may be impacted by atmospheric interference
Monitoring of WQPs on large spatiotemporal scale coverage	Accuracy may be impacted by the resolution
Cost and labor effective	Requires knowledge of data processing and analysis
Repository of historical images for water quality studies	Requires high-spec computer for large download and storage

The strengths and drawbacks are further explained in the following paragraphs below:

Strengths

RS applications allow for the monitoring of WQPs including TDS and TSS on a large spatiotemporal scale. With RS, changes in these WQPs are monitored over time and across large areas and at a great distance ranging from hundreds to thousands of miles compared to grab sampling approaches which are point specific. Additionally, RS can facilitate the study of these WQPs in areas that are hard to access or inaccessible, such as remote, dangerous, or politically sensitive areas. RS also makes it easy to identify sources, routes, and sinks of sediments and other parameters in water bodies in these areas [2,13,36,124,239].

RS images used for monitoring these WQPS range from low, to moderate to high-resolution obtained from Landsat, RapidEye, SPOT, MODIS, MERIS, the Advanced Wide Field Sensor (AWiFS), and Sentinel-2 among many others. A high spatial resolution image captured allows for accurate detection of TDS and TSS comparable with conventional methods [2,34,36,40,127,134,190].

Most RS images are publicly accessible, open-source data that users can obtain for free or at a low cost. Some of these images such as those of Landsat can date back as far as the 1970s and have been used extensively for the estimation of TSS and TDS in several studies possibly due to the fact they are easily accessible and come at little to no cost. RS applications aid in reducing associated cost-intensive laboratory equipment and reagents [167,189,200,239]. By using Landsat image data, users have saved around USD 3.45 billion as of 2017, with users in the United States making up more than half of that total [261]. Landsat imagery has been used in historical as well as contemporary regional assessments of various WQPs to assess water clarity [262].

When used in conjunction with conventional field measurements, RS can be used to develop algorithms and models for accurate estimations of TDS and TSS concentrations even in remote and inaccessible areas and in real-time. Additionally, conventional methods of measurement are susceptible to errors caused by sample storage, transportation, and analysis which can be reduced with the RS application. RS thus offers a non-invasive mechanism that does not require physical water sampling, hence cutting errors associated with sample storage, transportation, and analysis [2,189,251].

Drawbacks

RS applications in the retrieval of WQPs such as TDS and TSS can be quite challenging, particularly in shallow waters where the retrieved parameter levels could be greatly influenced by the contribution of the benthic signal to the overall reflectance signal, requiring the need for specific correction algorithms which consider the influence of the bottom reflectance to improve the accuracy of the WQP estimations. Other factors of the shallow water bodies which could also impact the accuracy of retrieval of the TDS and TSS include the varied bottom depths, types, and substrates which have the potential to impact the scattering and absorptive characteristics of light signals [263,264]. The accuracy of these retrieved WQPs in transitional waters such as estuaries could also be less successful owing to the high optical complexities of these waters coupled with their closeness to the land [93]. Additionally, the accuracy of data acquired might be affected by atmospheric factors such as cloud cover and haze, which are serious drawbacks of using RS for monitoring WQPs such as TDS and TSS. It is much more difficult to obtain accurate data with RS technologies in regions that have regular cloud cover or significant levels of air pollution [2,124,265].

RS may not always produce the level of detail needed for precise TDS and TSS measurements since the resolution of the imagery and data collected can be limited by the altitude of the platform used for the data collection which can present challenges to monitoring and measuring parameters such as TDS and TSS in water bodies with intricate shorelines or highly localized areas [266].

Another drawback with the use of RS in the measurement of TDS and TSS is the difficulty in making distinctions between these components of total solids. TSS is an optically active parameter that can be easily detected with optical sensors, TDS on the hand is difficult to accurately obtain from RS platforms. They are estimated from RS images because of their relationships with colored WQPs with which they may co-vary [2,36,267].

Although most RS images are available at no cost there are some images particularly hyperspectral images that require payment for the use of images. The associated cost of airborne sensors mounted on aircraft to acquire RS images may be significantly high and can deter other people from having access to such technologies. The initial cost of equipment and training for RS technology can be high. This may make them inaccessible to smaller organizations or underfunded researchers particularly those in developing countries [124,266].

RS applications in WQPs measurement require specialized training to analyze the images and data gathered. Individuals using RS in monitoring and measuring WQPs such as TDS and TSS require expertise in the use of software such as ArcGIS and Google Earth Engine among others, which can limit the number of people who can utilize these applications [46,132,266].

Another limitation of RS applications is the spatial, temporal, and spectral resolutions of the sensor used in the data collection. It may be challenging to rely on a certain RS sensor with a longer repeat cycle to detect temporal variations in the TDS and TSS. RS sensors offer a variety of spatial, spectral, and temporal resolutions. One example is contrasting the temporal resolutions of Landsat 8 OLI and Sentinel-2 A/B MSI, both of which have revisit times of 16 days and 5 days, respectively [2,268].

The last but not the least limitation of RS techniques in estimating WQPs such as TDS and TSS, is the lack of field data for the calibration and validation of the models developed with RS data due to the high cost of on-site sampling and the required expertise in analyzing and making inferences from the samples collected. These issues are more prevalent in Sub-Saharan Africa which has less expertise and technology. The lack of proper calibration and validation of remote sensed models exposes the accuracy of these models to questioning [2,7,10,36].

5. Conclusions and Recommendations

TDS and TSS concentrations or loads in a water body play a significant role in the management and sustainability of water resources. Increased TDS may affect the taste of drinking water and can also cause scaling and corrosion of pipes and other water systems. It can reduce the efficacy of water treatment systems, raising the cost of operating these facilities. An increase in TSS on the other hand, affects the optical clarity of the water and hence impacts the rate of photosynthesis of aquatic organisms. Monitoring and managing these water quality indicators is therefore key to reducing the adverse consequences on human and aquatic health, and the environment, and to ensuring the sustainability of the water resource.

Monitoring of TDS and TSS can be achieved through conventional and RS methods. Conventional methods such as field sampling and gravimetric analysis determining TDS and TSS have been in use for a long time and are still crucial for monitoring these WQPs. Conventional methods are standardized, straightforward, and validated over time, offering consistent and reliable measurement. Monitoring conventionally, however, presents limitations. Field sampling and gravimetric analysis are labor and cost-intensive and require a lot of time. They are also limited in space and time. RS techniques and geospatial tools offer an economical method for determining TDS and TSS on a large spatial scale in an accurate manner in both space and time. RS sensors categorized as airborne and spaceborne have been used to capture images for the retrieval and estimation of WQPs such as TSS and TDS. While TSS is optically active and can be sensed directly from these sensors, TDS is an optically inactive parameter whose determination is based on its association with other WQPs with which it may co-vary [2]. The reflectance in the 580–900 nm region of the electromagnetic spectrum has been reported to be most sensitive to TSS concentration changes and hence most ideal for its retrieval [124,149,269].

Estimations and retrieval of these parameters are widely performed using empirical, analytical, semi-empirical models, and more recently, through advanced models in the form of AI or ML models. The choice of a particular image from the sensors to be used depended on several factors including associated cost, and spectral, temporal, and spatial, resolutions [2]. These models could present some errors due to the coarse resolutions of the images. An example is the use of coarse 250 m resolution MODIS data for a study of small inland water bodies. A study by researchers [232] compared the Chinese high-resolution GF-1 Wide Field Imager (WFI) data with MODIS for the estimation of suspended particulate matter and found that the GF-1 was able to resolve over 75% of the spatial variations, whereas the MODIS band with 250 m resolution could only detect 40% of them, demonstrating the drawbacks of employing such coarse resolution images. The issues of temporal, spectral, and spatial resolution associated with images in RS are addressed with recent advancements and increment of UAV airborne captured images [2].

Another limitation of RS methods is the issue of atmospheric interference on the captured images, introducing errors in the retrieval of the WQPs. Studies have, however, suggested several models including the Dark Object Subtraction (DOS), Polynomial-based algorithm applied to MERIS (Polymer), Sentinel 2 Correction (Sen2Cor), correction for atmospheric effects (iCOR), The standard NASA atmospheric correction (NASA-AC), and Atmospheric correction for OLI 'lite' (ACOLITE) models, the Rayleigh-corrected reflectance algorithms among others minimize associated errors [2,101,270]. Hyperspectral RS inversion models could also be used in retrieving the optical properties when dealing with shallow waters to improve the accuracy of the results [263].

Additionally, the presence of different constituents including CDOM, NAP, and phytoplankton at different concentrations in inland waters has made the determination of WQPs such as TSS and TDS in inland waters more challenging and less effective as compared to open oceans [6]. There is also a need for testing and training of developed models using in situ field measurements to improve the accuracy of their predictions.

For effective monitoring and management of TDS and TSS in water bodies using RS applications, the following recommendations are proposed:

1. Fusion or combination of bands from different sensors: the fusion of microwave and optical bands should be explored in the estimation of TDS and TSS in water bodies. The fusion of data from optical bands and ERS-2 SAR bands could increase the performance in the retrieval of WQPs such as TDS and TSS concentrations in water systems. There have been significant successes in the use of microwave domain radiometers and synthetic aperture radars in the estimation of surface salinity in coastal water systems. In a study [179] comparing the MODIS-Landsat fusion results to single-band algorithms for TSS estimations, the fusion model performed better in TSS estimations in dynamic river systems than the single-band MODIS model because it had finer spatial resolution. The reported R^2 for the MODIS-based model increased from 65–77% to 85–89% for the Landsat-MODIS fused model [179].
2. Utilization of ML and AI Algorithms for the retrieval and estimation of WQPS: instead of utilizing empirical approaches, estimation, retrieval, and interpretation of TDS and TSS concentrations from RS data should use ML techniques. Despite being simple to use and requiring less computation time and effort than other methods, empirical methods of retrieval may not be able to distinguish these WQPs. To increase the

accuracy of WQPs retrieved using RS, ML models including ANN and SVM that have the potential to reflect complex nonlinear models through training and testing should be utilized [2,24,192].

3. Observed or ground-truth data from conventional field sampling should be used to complement RS measurements: this is important to ensure proper calibration and validation of RS models. Statistical or evaluation metrics such as the R^2, Percent Bias (PBIAS), MAE, NSE, RMSE, and the ratio of the RMSE to standard deviation which have been widely used should be utilized to evaluate developed models to improve their accuracy and robustness [2,128,145,271–277].
4. Remote sensed retrieval and estimation of TDS and TSS should be using high-resolution images where practical and possible: for accurate and effective detection of these WQPs by remote sensing, a high-resolution image with frequent revisit times should be used to ensure a timely change in these parameters are adequately captured. Images from GeoEye IKONOS, which has a spatial resolution of 0.82–5 m with a revisit interval of 2–3 days, and Digital Globe WorldView-1, which has a resolution of 0.5 m and a revisit period of 1.7 days, are two examples of high-resolution satellite images which could be used for the effective retrieval and estimations of TDS and TSS. Hyperspectral and high-resolution imageries such as images from the Hyperspectral Digital Imagery Collection Experiment by the Naval Research Lab, Airborne Imaging Spectrometer Multispectral by Spectral Imaging, and the AVIRIS by the NASA Jet Propulsion Laboratory could aid in the elimination of issues of discrete spectral signatures associated with other images. Hyperspectral and high-resolution images have a high potential of effectively discriminating changes in TSS and TDS in water bodies [2].
5. Applying atmospheric corrections when using level 1 satellite images: atmospheric corrections such as DOS, Polymer, Sen2Cor, iCOR, NASA-AC, and ACOLITE should be employed in minimizing errors associated with atmospheric interferences on the satellite images to ultimately improve the accuracy of the WQP retrievals [2,270].

In conclusion, as water bodies are continuing to be impaired by anthropogenic activities and changes in climate, the importance of continued water quality monitoring should not be overlooked. There should be continuous exploration and investigation of forward-thinking ideas for research in the monitoring of WQPs such as TDS and TSS using conventional and RS techniques. While this research offers a thorough overview of the various applications for measuring TDS and TSS in the water body, there are several directions for further study in TDS and TSS measurement particularly with RS measurements.

Some of these areas of possible future research and exploration include the development of new technology and sensors that can offer real-time in situ monitoring of TDS and TSS. These technologies can enable quick responses to changes in water quality and help to increase the effectiveness and accuracy of water quality monitoring.

Another area of future research is the integration of multiple RS data, such as the use of both satellite and UAV data to provide comprehensive and detailed information on the water bodies for accurate measurements. The UAV provides hyperspectral images with finer spatial resolution, which has the potential to improve the overall performance of models used in estimating TDS and TSS.

Further investigation is also required into the potential effects of anthropogenic and natural factors on TDS and TSS levels in water bodies, as well as how these factors can be considered in conventional measurements and RS techniques. Additionally, there is a need for further research to develop novel RS algorithms that can efficiently and accurately estimate TDS and TSS in real-time to facilitate rapid responses to the changes in the state of water caused by changes in these WQPs.

This review provides conventional and RS approaches which could be applied to the monitoring and management of water resources. This comprehensive review offers stakeholders and decision-makers a go-to repository to enhance their monitoring efforts assessments and mitigation of water quality impairments. Regulatory bodies could also rely on this repository to aid in developing effective regulations to enhance monitoring efforts.

Author Contributions: G.E.A. contributed to the conceptualization, methodology, and original and final writing of the manuscript. H.S. and S.A. both contributed to the conceptualization and writing—review and editing, and supervision of the manuscript. D.J. contributed to the writing—review, editing, technical support, and supervision of the manuscript. All authors have read and agreed to the published version of the manuscript.

Funding: This research received no external funding.

Data Availability Statement: This work relied on published materials and public platforms, which have been duly referenced.

Conflicts of Interest: The authors declare no conflict of interest.

Appendix A. Landsat Band Designations

Table A1. Band specifications for Landsat 8 OLI with wavelength, spatial resolution, and signal-to-noise ratio (S/N) scaled for radiances. Adapted from [207–209].

Band	S/N	Wavelength (μm)	Spatial Resolution (m)
Band 1–Coastal aerosol	284	0.43–0.45	30
Band 2–Blue	321	0.45–0.51	30
Band 3–Green	223	0.53–0.59	30
Band 4–Red	113	0.64–0.67	30
Band 5–NIR *	45	0.85–0.88	30
Band 6–SWIR 1 *	10.1	1.57–1.65	30
Band 7–SWIR 2 *	7.4	2.11–2.29	30
Band 8–Panchromatic		0.50–0.68	15
Band 9–Cirrus		1.36–1.38	30

* NIR = Near Infrared. * SWIR = Short Wave Infrared.

Table A2. Band specifications for Landsat 7 ETM+ with wavelength and spatial resolution. Adapted from [149,207,208].

Band	Wavelength (μm)	Spatial Resolution (m)
Band 1–Blue	0.45–0.52	30
Band 2–Green	0.52–0.60	30
Band 3–Red	0.63–0.69	30
Band 4-NIR *	0–77–0.90	30
Band 5–SWIR * 1	1.55–1.75	30
Band 6–Thermal	10.40–12.50	60 (*30)
Band 7–SWIR * 2	2.09–2.35	30
Band 8–Panchromatic	0.52–0.90	15

* NIR = Near Infrared. * SWIR = Short Wave Infrared. *30 = 60 m spatial resolution resampled to 30 m.

Table A3. Band specifications for Landsat 5 ETM with wavelength and spatial resolution. Adapted from [207,238].

Band	Wavelength (μm)	Spatial Resolution (m)
Band 1–Blue	0.45–0.52	30
Band 2–Green	0.53–0.61	30
Band 3–Red	0.63–0.69	30
Band 4-NIR *	0.76–0.90	30
Band 5–SWIR * 1	1.55–1.75	30
Band 6–Thermal	10.40–12.50	120
Band 7–SWIR * 2	0.08–2.35	30

* NIR = Near Infrared. * SWIR = Short Wave Infrared.

Appendix B. Sentinel-2 MSI Band Designations

Table A4. Band specifications for Sentinel-2 MSI with band center, S/N, and spatial resolution scaled for radiances. Adapted from [209,211,278].

Band	S2A			S2B		
	S/N	Wavelength (nm)	Bandwidth (nm)	Wavelength (nm)	Bandwidth (nm)	Spatial Resolution (m)
B2-Blue	102	492.4	66	492.1	66	10
B3-Green	79	559.8	36	559.0	36	
B4-Red	45	664.6	31	664.9	31	
B8-NIR *	20	832.8	106	832.9	106	
B5-Red Edge 1	45	704.1	15	703.8	16	20
B6-Red Edge 2	34	740.5	15	739.1	15	
B7-Red Edge 3	26	782.8	20	779.7	20	
B8a-Red Edge 4	16	864.7	21	864.0	22	
B11-SWIR * 1	2.8	1613.7	91	1610.4	94	
B12-SWIR * 2	2.2	2202.4	175	2185.7	185	
B1-Aerosols	439	442.7	21	442.2	21	60
B9-Water vapor		945.1	20	943.2	21	
B10-Cirrus		1373.5	31	1376.9	30	

* NIR = Near Infrared. * SWIR = Short Wave Infrared.

References

1. Khan, I.; Khan, A.; Khan, M.S.; Zafar, S.; Hameed, A.; Badshah, S.; Rehman, S.U.; Ullah, H.; Yasmeen, G. Impact of City Effluents on Water Quality of Indus River: Assessment of Temporal and Spatial Variations in the Southern Region of Khyber Pakhtunkhwa, Pakistan. *Environ. Monit. Assess.* **2018**, *190*, 267. [CrossRef] [PubMed]
2. Adjovu, G.E.; Stephen, H.; James, D.; Ahmad, S. Overview of the Application of Remote Sensing in Effective Monitoring of Water Quality Parameters. *Remote Sens.* **2023**, *15*, 1938. [CrossRef]
3. Adjovu, G.E.; Stephen, H.; Ahmad, S. Spatial and Temporal Dynamics of Key Water Quality Parameters in a Thermal Stratified Lake Ecosystem: The Case Study of Lake Mead. *Earth* **2023**, *4*, 461–502. [CrossRef]
4. American Public Health Association; American Water Works Association; Water Environment Federation. *Standard Methods for the Examination of Water and Wastewater*; Baird, R.B., Eaton, A.D., Rice, E.W., Eds.; American Public Health Association: Washington, DC, USA; American Water Works Association: Denver, CO, USA; Water Environment Federation: Alexandria, VA, USA, 2017; ISBN 9788578110796.
5. Standard Methods Committee; Wilder, B.H.; Costa, H.S.; Kosmowski, C.M.; Purcell, W.E. Methods 2540. Available online: http://edgeanalytical.com/wp-content/uploads/Waste_SM2540.pdf (accessed on 2 July 2023).
6. Ogashawara, I.; Mishra, D.R.; Gitelson, A.A. *Remote Sensing of Inland Waters: Background and Current State-of-the-Art*; Elsevier Inc.: Amsterdam, The Netherlands, 2017; ISBN 9780128046548.
7. Dey, J.; Vijay, R. A Critical and Intensive Review on Assessment of Water Quality Parameters through Geospatial Techniques. *Environ. Sci. Pollut. Res.* **2021**, *28*, 41612–41626. [CrossRef]
8. Dörnhöfer, K.; Oppelt, N. Remote Sensing for Lake Research and Monitoring—Recent Advances. *Ecol. Indic.* **2016**, *64*, 105–122. [CrossRef]
9. Cheng, C.; Zhang, F.; Shi, J.; Kung, H.T. What Is the Relationship between Land Use and Surface Water Quality? A Review and Prospects from Remote Sensing Perspective. *Environ. Sci. Pollut. Res.* **2022**, *29*, 56887–56907. [CrossRef] [PubMed]
10. Dube, T.; Mutanga, O.; Seutloali, K.; Adelabu, S.; Shoko, C. Water Quality Monitoring in Sub-Saharan African Lakes: A Review of Remote Sensing Applications. *Afr. J. Aquat. Sci.* **2015**, *40*, 1–7. [CrossRef]
11. Giao, N.T.; Van Cong, N.; Nhien, H.T.H. Using Remote Sensing and Multivariate Statistics in Analyzing the Relationship between Land Use Pattern and Water Quality in Tien Giang Province, Vietnam. *Water* **2021**, *13*, 1093. [CrossRef]
12. Karaoui, I.; Arioua, A.; Boudhar, A.; Hssaisoune, M.; Mouatassime, S.E.; Ouhamchich, K.A.; Elhamdouni, D. Evaluating the Potential of Sentinel-2 Satellite Images for Water Quality Characterization of Artificial Reservoirs: The Bin El Ouidane Reservoir Case Study (Morocco). *Karaoui Ismail Arioua Abdelkrim Abdelghani Boudhar Hssaisoune Mohammed Sabri* **2019**, *7*, 31–39.
13. Nath, R.K.; Deb, S.K. Water-Body Area Extraction From High Resolution Satellite Images-An Introduction, Review, and Comparison. *Int. J. Image Process.* **2010**, *3*, 353–372.
14. Palmer, S.C.J.; Kutser, T.; Hunter, P.D. Remote Sensing of Inland Waters: Challenges, Progress and Future Directions. *Remote Sens. Environ.* **2015**, *157*, 1–8. [CrossRef]
15. Song, K. Water Quality Monitoring Using Landsat Thematе Mapper Data with Empirical Algorithms in Chagan Lake, China. *J. Appl. Remote Sens.* **2011**, *5*, 053506. [CrossRef]

16. Zhou, Y.; Dong, J.; Xiao, X.; Xiao, T.; Yang, Z.; Zhao, G.; Zou, Z.; Qin, Y. Open Surface Water Mapping Algorithms: A Comparison of Water-Related Spectral Indices and Sensors. *Water* **2017**, *9*, 256. [CrossRef]
17. Lemessa, F.; Simane, B.; Seyoum, A.; Gebresenbet, G. Assessment of the Impact of Industrial Wastewater on the Water Quality of Rivers around the Bole Lemi Industrial Park (BLIP), Ethiopia. *Sustainability* **2023**, *15*, 4290. [CrossRef]
18. Adjovu, G.E.; Stephen, H.; Ahmad, S. Spatiotemporal Variability in Total Dissolved Solids and Total Suspended Solids along the Colorado River. *Hydrology* **2023**, *10*, 125. [CrossRef]
19. Gootman, K.S.; Hubbart, J.A. Characterization of Sub-Catchment Stream and Shallow Groundwater Nutrients and Suspended Sediment in a Mixed Land Use, Agro-Forested Watershed. *Water* **2023**, *15*, 233. [CrossRef]
20. Al-Mahasneh, M.; Al Bsoul, A.; Al-Ananzeh, N.; Al-Khasawane, H.E.; Al-Mahasneh, M.; Tashtoush, R. The Characterization of Groundwater Quality for Safe Drinking Water Wells via Disinfection and Sterilization in Jordan: A Case Study. *Hydrology* **2023**, *10*, 135. [CrossRef]
21. Azzirgue, E.M.; Cherif, E.K.; El Azhari, H.; Dakak, H.; Yachou, H.; Ghanimi, A.; Nouayti, N.; Esteves da Silva, J.; Salmoun, F. Interactions Evaluation between the Jouamaa Hakama Groundwater and Ouljat Echatt River in the North of Morocco, Using Hydrochemical Modeling, Multivariate Statistics and GIS. *Water* **2023**, *15*, 1752. [CrossRef]
22. Schliemann, S.A.; Grevstad, N.; Brazeau, R.H. Water Quality and Spatio-Temporal Hot Spots in an Effluent-Dominated Urban River. *Hydrol. Process.* **2021**, *35*, e14001. [CrossRef]
23. Buma, W.G.; Lee, S.I. Evaluation of Sentinel-2 and Landsat 8 Images for Estimating Chlorophyll-a Concentrations in Lake Chad, Africa. *Remote Sens.* **2020**, *12*, 2437. [CrossRef]
24. Vakili, T.; Amanollahi, J. Determination of Optically Inactive Water Quality Variables Using Landsat 8 Data: A Case Study in Geshlagh Reservoir Affected by Agricultural Land Use. *J. Clean. Prod.* **2020**, *247*, 119134. [CrossRef]
25. Zhang, X.; Fichot, C.G.; Baracco, C.; Guo, R.; Neugebauer, S.; Bengtsson, Z.; Ganju, N.; Fagherazzi, S. Determining the Drivers of Suspended Sediment Dynamics in Tidal Marsh-Influenced Estuaries Using High-Resolution Ocean Color Remote Sensing. *Remote Sens. Environ.* **2020**, *240*, 111682. [CrossRef]
26. Leggesse, E.S.; Zimale, F.A.; Sultan, D.; Enku, T.; Srinivasan, R.; Tilahun, S.A. Predicting Optical Water Quality Indicators from Remote Sensing Using Machine Learning Algorithms in Tropical Highlands of Ethiopia. *Hydrology* **2023**, *10*, 110. [CrossRef]
27. Shaikh, T.A.; Adjovu, G.E.; Stephen, H.; Ahmad, S. Impacts of Urbanization on Watershed Hydrology and Runoff Water Quality of a Watershed: A Review. In Proceedings of the World Environmental and Water Resources Congress 2023, Henderson, NV, USA, 21–25 May 2023; Volume 1, pp. 1271–1283.
28. Leigh, C.; Kandanaarachchi, S.; McGree, J.M.; Hyndman, R.J.; Alsibai, O.; Mengersen, K.; Peterson, E.E. Predicting Sediment and Nutrient Concentrations from High-Frequency Water-Quality Data. *PLoS ONE* **2019**, *14*, e0215503. [CrossRef]
29. Dritsas, E.; Trigka, M. Efficient Data-Driven Machine Learning Models for Water Quality Prediction. *Computation* **2023**, *11*, 16. [CrossRef]
30. Avila, R.; Horn, B.; Moriarty, E.; Hodson, R.; Moltchanova, E. Evaluating Statistical Model Performance in Water Quality Prediction. *J. Environ. Manag.* **2018**, *206*, 910–919. [CrossRef] [PubMed]
31. Fant, C.; Srinivasan, R.; Boehlert, B.; Rennels, L.; Chapra, S.C.; Strzepek, K.M.; Corona, J.; Allen, A.; Martinich, J. Climate Change Impacts on US Water Quality Using Two Models: HAWQS and US Basins. *Water* **2017**, *9*, 118. [CrossRef]
32. Lee, S.; Ahn, K.H. Monitoring of COD as an Organic Indicator in Waste Water and Treated Effluent by Fluorescence Excitation-Emission (FEEM) Matrix Characterization. *Water Sci. Technol.* **2004**, *50*, 57–63. [CrossRef]
33. Serafy, G.Y.H.E.; Schaeffer, B.A.; Neely, M.; Spinosa, A.; Odermatt, D.; Weathers, K.C.; Baracchini, T.; Bouffard, D.; Carvalho, L.; Conmy, R.N.; et al. Integrating Inland and Coastal Water Quality Data for Actionable Knowledge. *Remote Sens.* **2021**, *13*, 2899. [CrossRef]
34. Zhao, J.; Zhang, F.; Chen, S.; Wang, C.; Chen, J.; Zhou, H.; Xue, Y. Remote Sensing Evaluation of Total Suspended Solids Dynamic with Markov Model: A Case Study of Inland Reservoir across Administrative Boundary in South China. *Sensors* **2020**, *20*, 6911. [CrossRef]
35. U.S. Environmental Protection Agency. *NPDES Compliance Inspection Manual—Chapter 5—Sampling*; U.S. Environmental Protection Agency, Office of Water, Office of Water Enforcement and Permits: Washington, DC, USA, 2017.
36. Gholizadeh, M.H.; Melesse, A.M.; Reddi, L. A Comprehensive Review on Water Quality Parameters Estimation Using Remote Sensing Techniques. *Sensors* **2016**, *16*, 1298. [CrossRef] [PubMed]
37. Adjovu, G.E.; Ali Shaikh, T.; Stephen, H.; Ahmad, S. Utilization of Machine Learning Models and Satellite Data for the Estimation of Total Dissolved Solids in the Colorado River System. In Proceedings of the World Environmental and Water Resources Congress 2023, Henderson, NV, USA, 21–25 May 2023; American Society of Civil Engineers: Henderson, NV, USA, 2023; Volume 1, pp. 1147–1160.
38. Hach Solids (Total & Dissolved). Available online: https://www.hach.com/parameters/solids (accessed on 8 June 2023).
39. O'Connor, D.J. Seasonal and Long-Term Variations of Dissolved Solids in Lakes and Reservoirs. *J. Environ. Eng.* **1989**, *115*, 1213–1234. [CrossRef]
40. Doxaran, D.; Froidefond, J.-M.; Lavender, S.; Castaing, P. Spectral Signature of Highly Turbid Waters. *Remote Sens. Environ.* **2002**, *81*, 149–161. [CrossRef]
41. Chawla, I.; Karthikeyan, L.; Mishra, A.K. A Review of Remote Sensing Applications for Water Security: Quantity, Quality, and Extremes. *J. Hydrol.* **2020**, *585*, 124826. [CrossRef]

42. Crotts, A. An Experimental Technique in Lowering Total Dissolved Solids in Wastewater. Bachelor's Thesis, University of Nevada Las Vegas, Las Vegas, NV, USA, 1996. [CrossRef]
43. McCleskey, R.B.; Cravotta, C.A.; Miller, M.P.; Tillman, F.; Stackelberg, P.; Knierim, K.J.; Wise, D.R. Salinity and Total Dissolved Solids Measurements for Natural Waters: An Overview and a New Salinity Method Based on Specific Conductance and Water Type. *Appl. Geochem.* **2023**, *154*, 105684. [CrossRef]
44. Hossain, A.K.M.A.; Mathias, C.; Blanton, R. Remote Sensing of Turbidity in the Tennessee River Using Landsat 8 Satellite. *Remote Sens.* **2021**, *13*, 3785. [CrossRef]
45. Nauman, T.W.; Ely, C.P.; Miller, M.P.; Duniway, M.C. Salinity Yield Modeling of the Upper Colorado River Basin Using 30-m Resolution Soil Maps and Random Forests. *Water Resour. Res.* **2019**, *55*, 4954–4973. [CrossRef]
46. Sagan, V.; Peterson, K.T.; Maimaitijiang, M.; Sidike, P.; Sloan, J.; Greeling, B.A.; Maalouf, S.; Adams, C. Monitoring Inland Water Quality Using Remote Sensing: Potential and Limitations of Spectral Indices, Bio-Optical Simulations, Machine Learning, and Cloud Computing. *Earth-Sci. Rev.* **2020**, *205*, 103187. [CrossRef]
47. Fondriest Environmental Inc. Conductivity, Salinity & Total Dissolved Solids-Environmental Measurement Systems. Available online: https://www.fondriest.com/environmental-measurements/parameters/water-quality/conductivity-salinity-tds/ (accessed on 12 July 2023).
48. Hayden, L.; Wood, J.; Hassell, S.; Jones, A.; Deese, A. Water-Quality Assessment of the Pasquotank River Watershed; Analysis of Dissolved Oxygen, PH, Salt, Total Dissolved Solids, and Conductivity. Available online: http://nia.ecsu.edu/ureomps2011/teams/ptank/PQT%20IEEE%20PAPER.pdf (accessed on 12 July 2023).
49. Butler, B.A.; Ford, R.G. Evaluating Relationships between Total Dissolved Solids (TDS) and Total Suspended Solids (TSS) in a Mining-Influenced Watershed. *Mine Water Environ.* **2018**, *31*, 18–30. [CrossRef]
50. Mueller, J.S.; Grabowski, T.B.; Brewer, S.K.; Worthington, T.A. Effects of Temperature, Total Dissolved Solids, and Total Suspended Solids on Survival and Development Rate of Larval Arkansas River Shiner. *J. Fish Wildl. Manag.* **2017**, *8*, 79–88. [CrossRef]
51. Wright, B.W.G.; Simon, W.; Bove, D.J.; Mast, M.A.; Leib, K.J. Distribution of PH Values and Dissolved Trace-Metal Concentrations in Streams Mining in the Animas River Watershed, San Juan County, Colorado Professional Paper 1651. *Integr. Investig. Environ. Eff. Hist. Min. Animas River Watershed San Juan Cty. Color* **2007**, *1651*, 497–541.
52. U.S. EPA. 2018 Edition of the Drinking Water Standards and Health Advisories Tables. Available online: https://www.epa.gov/system/files/documents/2022-01/dwtable2018.pdf (accessed on 29 June 2023).
53. *EPA 816-F-09-004*; U.S. EPA National Primary Drinking Water Guidelines. United States Environmental Protection Agency: Washington, DC, USA, 2009; 7p.
54. Mejía Ávila, D.; Torres-Bejarano, F.; Martínez Lara, Z. Spectral Indices for Estimating Total Dissolved Solids in Freshwater Wetlands Using Semi-Empirical Models. A Case Study of Guartinaja and Momil Wetlands. *Int. J. Remote Sens.* **2022**, *43*, 2156–2184. [CrossRef]
55. Shareef, M.A.; Toumi, A.; Khenchaf, A. Estimating of Water Quality Parameters Using SAR and Thermal Microwave Remote Sensing Data. In Proceedings of the 2016 2nd International Conference on Advanced Technologies for Signal and Image Processing (ATSIP), Monastir, Tunisia, 21–23 March 2016; pp. 586–590. [CrossRef]
56. Shevah, Y. *1.4 Adaptation to Water Scarcity and Regional Cooperation in the Middle East*; Elsevier Ltd.: Amsterdam, The Netherlands, 2013; Volume 1, ISBN 9780123821829.
57. United States Geology Survey (USGS). Definition of "Brackish". Available online: https://ne.water.usgs.gov/ogw/review/brackish.html (accessed on 2 July 2023).
58. Nasreen. Ocean Salinity. *Int. J. Mod. Trends Sci. Technol.* **2022**, *8*, 296–302. [CrossRef]
59. Antonov, J.I.; Levitus, S. *World Ocean Atlas 2005*; The National Oceanic and Atmospheric Administration (NOAA): Washington, DC, USA, 2006; Volume 2.
60. Water Resources Mission Area. Brackish Groundwater Assessment. Available online: https://www.usgs.gov/mission-areas/water-resources/science/brackish-groundwater-assessment (accessed on 2 July 2023).
61. Godsey, W.E. Fresh, Brackish or Saline Water for Hydraulic Fracs: What Are the Options? Available online: https://www.epa.gov/sites/default/files/documents/02_Godsey_-_Source_Options_508.pdf (accessed on 2 July 2023).
62. Shapasand, M.; Alizadeh, A.R.; Yousefi, M.; Amini, J. Performance and Physiological Responses of Dairy Cattle to Water Total Dissolved Solids (TDS) under Heat Stress. *J. Appl. Anim. Res.* **2010**, *38*, 165–168. [CrossRef]
63. Usali, N.; Ismail, M.H. Use of Remote Sensing and GIS in Monitoring Water Quality. *J. Sustain. Dev.* **2010**, *3*, 228–238. [CrossRef]
64. Jones, J.R.; Knowlton, M.F. Suspended Solids in Missouri Reservoirs in Relation to Catchment Features and Internal Processes. *Water Res.* **2005**, *39*, 3629–3635. [CrossRef]
65. He, C.; Yao, Y.; Lu, X.; Chen, M.; Ma, W.; Zhou, L. Exploring the Influence Mechanism of Meteorological Conditions on the Concentration of Suspended Solids and Chlorophyll-a in Large Estuaries Based on MODIS Imagery. *Water* **2019**, *11*, 375. [CrossRef]
66. Walch, H.; von der Kammer, F.; Hofmann, T. Freshwater Suspended Particulate Matter—Key Components and Processes in Floc Formation and Dynamics. *Water Res.* **2022**, *220*, 118655. [CrossRef]
67. Ritchie, J.C.; Zimba, P.V.; Everitt, J.H. Remote Sensing Techniques to Assess Water Quality. *Photogramm. Eng. Remote Sens.* **2003**, *69*, 695–704. [CrossRef]

68. Azzam, A.; Uddin, H.; Mannan, U. Estimation of Suspended Sediment Concentration of Keenjhar Lake through Remote Sensing. In Proceedings of the 12th International Civil Engineering Conference (ICEC-2022), Karachi, Pakistan, 13–14 May 2022; p. 20.
69. US EPA. *Developing Water Quality Criteria for Suspended and Bedded Sediments (SABS)*; United States Environmental Protection Agency: Washington, DC, USA, 2019.
70. Karagiannis, I.C.; Soldatos, P.G. Water Desalination Cost Literature: Review and Assessment. *Desalination* **2008**, *223*, 448–456. [CrossRef]
71. Texas Water Development Board. Seawater FAQs Answers to Frequently Asked Questions. Available online: https://www.twdb.texas.gov/innovativewater/desal/faqseawater.asp#:~:text=1 (accessed on 12 July 2023).
72. Hintz, W.D.; Relyea, R.A. A Review of the Species, Community, and Ecosystem Impacts of Road Salt Salinisation in Fresh Waters. *Freshw. Biol.* **2019**, *64*, 1081–1097. [CrossRef]
73. Nguyen, K.A.; Liou, Y.A.; Tran, H.P.; Hoang, P.P.; Nguyen, T.H. Soil Salinity Assessment by Using Near-Infrared Channel and Vegetation Soil Salinity Index Derived from Landsat 8 OLI Data: A Case Study in the Tra Vinh Province, Mekong Delta, Vietnam. *Prog. Earth Planet. Sci.* **2020**, *7*, 1. [CrossRef]
74. Corwin, D.L.; Yemoto, K. Salinity: Electrical Conductivity and Total Dissolved Solids. *Soil Sci. Soc. Am. J.* **2020**, *84*, 1442–1461. [CrossRef]
75. Ladwig, R.; Rock, L.A.; Dugan, H.A. Impact of Salinization on Lake Stratification and Spring Mixing. *Limnol. Oceanogr. Lett.* **2021**, *8*, 93–102. [CrossRef]
76. Pessoa, L.G.M.; Freire, M.B.G.D.S.; Wilcox, B.P.; Green, C.H.M.; De Araújo, R.J.T.; De Araújo Filho, J.C. Spectral Reflectance Characteristics of Soils in Northeastern Brazil as Influenced by Salinity Levels. *Environ. Monit. Assess.* **2016**, *188*, 616. [CrossRef] [PubMed]
77. Figler, A.; B-Béres, V.; Dobronoki, D.; Márton, K.; Nagy, S.A.; Bácsi, I. Salt Tolerance and Desalination Abilities of Nine Common Green Microalgae Isolates. *Water* **2019**, *11*, 2527. [CrossRef]
78. Morshed, M.M.; Islam, M.T.; Jamil, R. Soil Salinity Detection from Satellite Image Analysis: An Integrated Approach of Salinity Indices and Field Data. *Environ. Monit. Assess.* **2016**, *188*, 119. [CrossRef]
79. Venkatesan, A.K.; Ahmad, S.; Johnson, W.; Batista, J.R. Salinity Reduction and Energy Conservation in Direct and Indirect Potable Water Reuse. *Desalination* **2011**, *272*, 120–127. [CrossRef]
80. Denys, L. Incomplete Spring Turnover in Small Deep Lakes in SE Michigan. *McNair Sch. Res. J.* **2010**, *2*, 10.
81. Bureau of Reclamation Quality of Water Progress Report No. 24. Available online: https://www.usbr.gov/uc/progact/salinity/pdfs/PR24final.pdf (accessed on 8 June 2023).
82. Tillman, F.D.; Day, N.K.; Miller, M.P.; Miller, O.L.; Rumsey, C.A.; Wise, D.R.; Longley, P.C.; McDonnell, M.C. A Review of Current Capabilities and Science Gaps in Water Supply Data, Modeling, and Trends for Water Availability Assessments in the Upper Colorado River Basin. *Water* **2022**, *14*, 3813. [CrossRef]
83. Shope, C.L.; Gerner, S.J. *Assessment of Dissolved-Solids Loading to the Colorado River in the Paradox Basin between the Dolores River and Gypsum Canyon Utah*; USA Department of the Interior; USA Geological Survey: Washington, DC, USA, 2016; pp. 1–18. [CrossRef]
84. Venkatesan, A.K.; Ahmad, S.; Johnson, W.; Batista, J.R. Systems Dynamic Model to Forecast Salinity Load to the Colorado River Due to Urbanization within the Las Vegas Valley. *Sci. Total Environ.* **2011**, *409*, 2616–2625. [CrossRef] [PubMed]
85. Mumme, S.P. The 1944 Water Treaty and the Incorporation of Environmental Values in U.S.-Mexico Transboundary Water Governance. *Environ. Sci. Policy* **2020**, *112*, 126–133. [CrossRef]
86. Tillman, F.D.; Anning, D.W. A Data Reconnaissance on the Effect of Suspended-Sediment Concentrations on Dissolved-Solids Concentrations in Rivers and Tributaries in the Upper Colorado River Basin. *J. Hydrol.* **2014**, *519*, 1020–1030. [CrossRef]
87. Venkatesan, A.K.; Ahmad, S.; Batista, J.R.; Johnson, W.S. Total Dissolved Solids Contribution to the Colorado River Associated with the Growth of Las Vegas Valley. In Proceedings of the World Environmental and Water Resources Congress 2010: Challenges of Change, Providence, RI, USA, 16–20 May 2010; pp. 3376–3385. [CrossRef]
88. Glysson, G.D.; Gray, J.R.; Schwarz, G.E. A Comparison of Load Estimates Using Total Suspended Solids and Suspended-Sediment Concentration Data. In Proceedings of the World Water and Environmental Resources Congress 2001, Orlando, FL, USA, 20–24 May 2001.
89. US EPA. *National Water Quality Inventory: Report to Congress*; Environmental Protection Agency: Washington, DC, USA, 2017.
90. Wang, M.; Chen, T.; Wang, X. Rapid Correction of Turbidity and CDOM Interference on Three-Dimensional Fluorescence Spectra of Live Algae Based on Deep Learning. *Photonics* **2023**, *10*, 627. [CrossRef]
91. Hidayati, N.F.; Rahman, M.; Fauzana, N.A.; Aisiah, S. Effectiveness of Chitosan To Reduce the Color Value, Turbidity, and Total Dissolved Solids in Shrimp-Washing Wastewater. *Russ. J. Agric. Socio-Econ. Sci.* **2021**, *115*, 82–88. [CrossRef]
92. Andreo, V.C.; Dogliotti, A.I.; Tauro, C.B. Remote Sensing of Phytoplankton Blooms in the Continental Shelf and Shelf-Break of Argentina: Spatio-Temporal Changes and Phenology. *IEEE J. Sel. Top. Appl. Earth Obs. Remote Sens.* **2016**, *9*, 5315–5324. [CrossRef]
93. Sent, G.; Biguino, B.; Favareto, L.; Cruz, J.; Sá, C.; Dogliotti, A.I.; Palma, C.; Brotas, V.; Brito, A.C. Deriving Water Quality Parameters Using Sentinel-2 Imagery: A Case Study in the Sado Estuary, Portugal. *Remote Sens.* **2021**, *13*, 1043. [CrossRef]
94. Dogliotti, A.I.; Ruddick, K.G.; Nechad, B.; Doxaran, D.; Knaeps, E. A Single Algorithm to Retrieve Turbidity from Remotely-Sensed Data in All Coastal and Estuarine Waters. *Remote Sens. Environ.* **2015**, *156*, 157–168. [CrossRef]
95. Dogliotti, A.I.; Ruddick, K.; Nechad, B.; Lasta, C.; Mercado, A. Calibration and Validation of an Algorithm for Remote Sensing of Turbidity Over La Plata River Estuary, Argentina. *EARSeL eProceedings* **2011**, *10*, 119–130.

96. Ruddick, K.; Vanhellemont, Q.; Dogliotti, A.I.; Nechad, B.; Pringle, N.; Van der Zande, D. New Opportunities and Challenges for High Resolution Remote Sensing of Water Colour. In Proceedings of the Ocean Optics XXIII, Victoria, BC, Canada, 23–28 October 2016.
97. Gokul, E.A.; Shanmugam, P.; Sundarabalan, B.; Sahay, A.; Chauhan, P. Modelling the Inherent Optical Properties and Estimating the Constituents' Concentrations in Turbid and Eutrophic Waters. *Cont. Shelf Res.* **2014**, *84*, 120–138. [CrossRef]
98. Nechad, B.; Ruddick, K.G.; Neukermans, G. Calibration and Validation of a Generic Multisensor Algorithm for Mapping of Turbidity in Coastal Waters. In *Proceedings of Remote Sensing of the Ocean, Sea Ice, and Large Water Regions 2009*; SPIE: Berlin, Germany, 2009.
99. Knaeps, E.; Dogliotti, A.I.; Raymaekers, D.; Ruddick, K.; Sterckx, S. In Situ Evidence of Non-Zero Reflectance in the OLCI 1020nm Band for a Turbid Estuary. *Remote Sens. Environ.* **2012**, *120*, 133–144. [CrossRef]
100. Camiolo, M.D.; Cozzolino, E.; Dogliotti, A.I.; Simionato, C.G.; Lasta, C.A. An Empirical Remote Sensing Algorithm for Retrieving Total Suspended Matter in a Large Estuarine Region. *Sci. Mar.* **2019**, *83*, 53–60. [CrossRef]
101. Dogliotti, A.I.; Ruddick, K.; Nechad, B.; Lasta, C. Estimating Turbidity in the La Plata River from MODIS Imagery. In Proceedings of the VI International Conference Current Problems in Optics of Natural Waters, St. Petersburg, Russia, 6–10 September 2011; pp. 1–8.
102. Imen, S.; Chang, N.B.; Yang, Y.J. Developing the Remote Sensing-Based Early Warning System for Monitoring TSS Concentrations in Lake Mead. *J. Environ. Manag.* **2015**, *160*, 73–89. [CrossRef] [PubMed]
103. Hajigholizadeh, M.; Moncada, A.; Kent, S.; Melesse, A.M. Land–lake Linkage and Remote Sensing Application in Water Quality Monitoring in Lake Okeechobee, Florida, USA. *Land* **2021**, *10*, 147. [CrossRef]
104. Sanjoto, T.B.; Elwafa, A.H.; Tjahjono, H.; Sidiq, W.A.B.N. Study of Total Suspended Solid Concentration Based on Doxaran Algorithm Using Landsat 8 Image in Coastal Water between Bodri River Estuary up to East Flood Canal Semarang City. *IOP Conf. Ser. Earth Environ. Sci.* **2020**, *561*, 012053. [CrossRef]
105. Edalat, M.M.; Stephen, H. Socio-Economic Drought Assessment in Lake Mead, USA, Based on a Multivariate Standardized Water-Scarcity Index. *Hydrol. Sci. J.* **2019**, *64*, 555–569. [CrossRef]
106. Cantwell, R.E.; Hofmann, R. Ultraviolet Absorption Properties of Suspended Particulate Matter in Untreated Surface Waters. *Water Res.* **2011**, *45*, 1322–1328. [CrossRef]
107. Mabwoga, S.O.; Chawla, A.; Thukral, A.K. Assessment of Water Quality Parameters of the Harike Wetland in India, a Ramsar Site, Using IRS LISS IV Satellite Data. *Environ. Monit. Assess.* **2010**, *170*, 117–128. [CrossRef] [PubMed]
108. Bid, S.; Siddique, G. Identification of Seasonal Variation of Water Turbidity Using NDTI Method in Panchet Hill Dam, India. *Model. Earth Syst. Environ.* **2019**, *5*, 1179–1200. [CrossRef]
109. Rusydi, A.F. Correlation between Conductivity and Total Dissolved Solid in Various Type of Water: A Review. *IOP Conf. Ser. Earth Environ. Sci.* **2018**, *118*, 012019. [CrossRef]
110. Chen, X.; Liu, L.; Zhang, X.; Li, J.; Wang, S.; Liu, D.; Duan, H.; Song, K. An Assessment of Water Color for Inland Water in China Using a Landsat 8-Derived Forel-Ule Index and the Google Earth Engine Platform. *IEEE J. Sel. Top. Appl. Earth Obs. Remote Sens.* **2021**, *14*, 5773–5785. [CrossRef]
111. Schaeffer, B.A.; Schaeffer, K.G.; Keith, D.; Lunetta, R.S.; Conmy, R.; Gould, R.W. Barriers to Adopting Satellite Remote Sensing for Water Quality Management. *Int. J. Remote Sens.* **2013**, *34*, 7534–7544. [CrossRef]
112. Kayhanian, M.; Suverkropp, C.; Ruby, A.; Tsay, K. Characterization and Prediction of Highway Runoff Constituent Event Mean Concentration. *J. Environ. Manag.* **2007**, *85*, 279–295. [CrossRef]
113. Fallatah, O.; Khattab, M.R. Evaluation of Groundwater Quality and Suitability for Irrigation Purposes and Human Consumption in Saudi Arabia. *Water* **2023**, *15*, 2352. [CrossRef]
114. Shareef, M.A.; Toumi, A.; Khenchaf, A. Estimation and Characterization of Physical and Inorganic Chemical Indicators of Water Quality by Using SAR Images. *SAR Image Anal. Model. Technol. XV* **2015**, *9642*, 96420U. [CrossRef]
115. Taylor, M.; Elliott, H.A.; Navitsky, L.O. Relationship between Total Dissolved Solids and Electrical Conductivity in Marcellus Hydraulic Fracturing Fluids. *Water Sci. Technol.* **2018**, *77*, 1998–2004. [CrossRef] [PubMed]
116. Pavelsky, T.M.; Smith, L.C. Remote Sensing of Suspended Sediment Concentration, Flow Velocity, and Lake Recharge in the Peace-Athabasca Delta, Canada. *Water Resour. Res.* **2009**, *45*, 1–16. [CrossRef]
117. Hasab, H.A.; Jawad, H.A.; Dibs, H.; Hussain, H.M.; Al-Ansari, N. Evaluation of Water Quality Parameters in Marshes Zone Southern of Iraq Based on Remote Sensing and GIS Techniques. *Water. Air. Soil Pollut.* **2020**, *231*, 183. [CrossRef]
118. Giardino, C.; Bresciani, M.; Braga, F.; Cazzaniga, I.; De Keukelaere, L.; Knaeps, E.; Brando, V.E. *Bio-Optical Modeling of Total Suspended Solids*; Elsevier Inc.: Amsterdam, The Netherlands, 2017; ISBN 9780128046548.
119. Wang, F.; Han, L.; Kung, H.T.; van Arsdale, R.B. Applications of Landsat-5 TM Imagery in Assessing and Mapping Water Quality in Reelfoot Lake, Tennessee. *Int. J. Remote Sens.* **2006**, *27*, 5269–5283. [CrossRef]
120. Chen, L.; Ling, F.; Bakker, G.; Liu, W.T.; Medema, G.; van der Meer, W.; Liu, G. Assessing the Transition Effects in a Drinking Water Distribution System Caused by Changing Supply Water Quality: An Indirect Approach by Characterizing Suspended Solids. *Water Res.* **2020**, *168*, 115159. [CrossRef]
121. Rieger, L.; Langergraber, G.; Thomann, M.; Fleischmann, N.; Siegrist, H. Spectral In-Situ Analysis of NO2, NO3, COD, DOC and TSS in the Effluent of a WWTP. *Water Sci. Technol.* **2004**, *50*, 143–152. [CrossRef] [PubMed]
122. Moeini, M.; Shojaeizadeh, A.; Geza, M. Supervised Machine Learning for Estimation of Total Suspended Solids in Urban Watersheds. *Water* **2021**, *13*, 147. [CrossRef]

123. Hach. Solids, Total Method 8271. Available online: https://images.hach.com/asset-get.download.jsa?id=7639984016 (accessed on 25 June 2023).
124. Yang, H.; Kong, J.; Hu, H.; Du, Y.; Gao, M.; Chen, F. A Review of Remote Sensing for Water Quality Retrieval: Progress and Challenges. *Remote Sens.* **2022**, *14*, 1770. [CrossRef]
125. US EPA. *Methods for Chemical Analysis of Water and Wastes*; Environmental Protection Agency: Washington, DC, USA, 1983.
126. Woodside, J. What Is the Difference among Turbidity, TDS, and TSS? Available online: https://www.ysi.com/ysi-blog/water-blogged-blog/2022/05/understanding-turbidity-tds-and-tss (accessed on 8 June 2023).
127. Adjovu, G.E.; Stephen, H.; Ahmad, S. Monitoring of Total Dissolved Solids Using Remote Sensing Band Reflectance and Salinity Indices: A Case Study of the Imperial County Section, AZ-CA, of the Colorado River. In Proceedings of the World Environmental and Water Resources Congress 2022, Atlanta, GA, USA, 5–8 June 2022. [CrossRef]
128. Pereira, O.J.R.; Merino, E.R.; Montes, C.R.; Barbiero, L.; Rezende-Filho, A.T.; Lucas, Y.; Melfi, A.J. Estimating Water PH Using Cloud-Based Landsat Images for a New Classification of the NhecolâNdia Lakes (Brazilian Pantanal). *Remote Sens.* **2020**, *12*, 1090. [CrossRef]
129. DeLuca, N.M.; Zaitchik, B.F.; Curriero, F.C. Can Multispectral Information Improve Remotely Sensed Estimates of Total Suspended Solids? A Statistical Study in Chesapeake Bay. *Remote Sens.* **2018**, *10*, 1393. [CrossRef]
130. Moore, G.K. Satellite Remote Sensing of Water Turbidity. *Hydrol. Sci. Bull.* **1980**, *25*, 407–421. [CrossRef]
131. Zhang, C.; Liu, Y.; Chen, X.; Gao, Y. Estimation of Suspended Sediment Concentration in the Yangtze Main Stream Based on Sentinel-2 MSI Data. *Remote Sens.* **2022**, *14*, 4446. [CrossRef]
132. Mohseni, F.; Saba, F.; Mirmazloumi, S.M.; Amani, M.; Mokhtarzade, M.; Jamali, S.; Mahdavi, S. Ocean Water Quality Monitoring Using Remote Sensing Techniques: A Review. *Mar. Environ. Res.* **2022**, *180*, 105701. [CrossRef]
133. Dekker, A.G.; Zamurovic, Ž.; Hoogenboom, H.J.; Peters, S.W.M. Remote Sensing, Ecological Water Quality Modelling and in Situ Measurements: A Case Study in Shallow Lakes. *Hydrol. Sci. J.* **1996**, *41*, 531–547. [CrossRef]
134. Wang, J.J.; Lu, X.X. Estimation of Suspended Sediment Concentrations Using Terra MODIS: An Example from the Lower Yangtze River, China. *Sci. Total Environ.* **2010**, *408*, 1131–1138. [CrossRef]
135. Kong, J.L.; Sun, X.M.; Wong, D.W.; Chen, Y.; Yang, J.; Yan, Y.; Wang, L.X. A Semi-Analytical Model for Remote Sensing Retrieval of Suspended Sediment Concentration in the Gulf of Bohai, China. *Remote Sens.* **2015**, *7*, 5373–5397. [CrossRef]
136. Jally, S.K.; Mishra, A.K.; Balabantaray, S. Retrieval of Suspended Sediment Concentration of the Chilika Lake, India Using Landsat-8 OLI Satellite Data. *Environ. Earth Sci.* **2021**, *80*, 298. [CrossRef]
137. Marinho, R.R.; Harmel, T.; Martinez, J.M.; Junior, N.P.F. Spatiotemporal Dynamics of Suspended Sediments in the Negro River, Amazon Basin, from in Situ and Sentinel-2 Remote Sensing Data. *ISPRS Int. J. Geo-Inf.* **2021**, *10*, 86. [CrossRef]
138. Novoa, S.; Doxaran, D.; Ody, A.; Vanhellemont, Q.; Lafon, V.; Lubac, B.; Gernez, P. Atmospheric Corrections and Multi-Conditional Algorithm for Multi-Sensor Remote Sensing of Suspended Particulate Matter in Low-to-High Turbidity Levels Coastal Waters. *Remote Sens.* **2017**, *9*, 61. [CrossRef]
139. Mao, Z.; Chen, J.; Pan, D.; Tao, B.; Zhu, Q. A Regional Remote Sensing Algorithm for Total Suspended Matter in the East China Sea. *Remote Sens. Environ.* **2012**, *124*, 819–831. [CrossRef]
140. Petus, C.; Chust, G.; Gohin, F.; Doxaran, D.; Froidefond, J.M.; Sagarminaga, Y. Estimating Turbidity and Total Suspended Matter in the Adour River Plume (South Bay of Biscay) Using MODIS 250-m Imagery. *Cont. Shelf Res.* **2010**, *30*, 379–392. [CrossRef]
141. Kupssinskü, L.S.; Guimarães, T.T.; De Souza, E.M.; Zanotta, D.C.; Veronez, M.R.; Gonzaga, L.; Mauad, F.F. A Method for Chlorophyll-a and Suspended Solids Prediction through Remote Sensing and Machine Learning. *Sensors* **2020**, *20*, 2125. [CrossRef]
142. Peterson, K.T.; Sagan, V.; Sidike, P.; Cox, A.L.; Martinez, M. Suspended Sediment Concentration Estimation from Landsat Imagery along the Lower Missouri and Middle Mississippi Rivers Using an Extreme Learning Machine. *Remote Sens.* **2018**, *10*, 1503. [CrossRef]
143. Najafzadeh, M.; Basirian, S. Evaluation of River Water Quality Index Using Remote Sensing and Artificial Intelligence Models. *Remote Sens.* **2023**, *15*, 2359. [CrossRef]
144. Alshehri, F.; Rahman, A. Coupling Machine and Deep Learning with Explainable Artificial Intelligence for Improving Prediction of Groundwater Quality and Decision-Making in Arid Region, Saudi Arabia. *Water* **2023**, *15*, 2298. [CrossRef]
145. Adjovu, G.E.; Stephen, H.; Ahmad, S. A Machine Learning Approach for the Estimation of Total Dissolved Solids Concentration in Lake Mead Using Electrical Conductivity and Temperature. *Water* **2023**, *15*, 2439. [CrossRef]
146. Kumar, D.N.; Reshmidevi, T.V. Remote Sensing Applications in Water Resources. *J. Indian Inst. Sci.* **2013**, *93*, 163–188.
147. Guo, H.; Huang, J.J.; Chen, B.; Guo, X.; Singh, V.P. A Machine Learning-Based Strategy for Estimating Non-Optically Active Water Quality Parameters Using Sentinel-2 Imagery. *Int. J. Remote Sens.* **2021**, *42*, 1841–1866. [CrossRef]
148. Ondrusek, M.; Stengel, E.; Kinkade, C.S.; Vogel, R.L.; Keegstra, P.; Hunter, C.; Kim, C. The Development of a New Optical Total Suspended Matter Algorithm for the Chesapeake Bay. *Remote Sens. Environ.* **2012**, *119*, 243–254. [CrossRef]
149. Allan, M.G.; Hicks, B.J.; Brabyn, L. *Remote Sensing of Water Quality in the Rotorua Lakes*; Centre for Biodiversity and Ecology Research, Department of Biological Sciences, School of Science and Engineering, The University of Waikato: Hamilton, New Zealand, 2007.
150. Allan, M.G.; Hamilton, D.P.; Hicks, B.J.; Brabyn, L. Landsat Remote Sensing of Chlorophyll a Concentrations in Central North Island Lakes of New Zealand. *Int. J. Remote Sens.* **2011**, *32*, 2037–2055. [CrossRef]

151. Uudeberg, K.; Aavaste, A.; Kõks, K.-L.; Ansper, A.; Uusõue, M.; Kangro, K.; Ansko, I.; Ligi, M.; Toming, K.; Reinart, A. Optical Water Type Guided Approach to Estimate Optical Water Quality Parameters. *Remote Sens.* **2020**, *12*, 931. [CrossRef]
152. Wojcik-Dugoborska, K.A.; Osinska, M.; Bialik, R.J. The Impact of Glacial Suspension Color on the Relationship between Its Properties and Marine Water Spectral Reflectance. *IEEE J. Sel. Top. Appl. Earth Obs. Remote Sens.* **2022**, *15*, 3258–3268. [CrossRef]
153. Ouni, H.; Kawachi, A.; Irie, M.; Ben M'Barek, N.; Hariga-Tlatli, N.; Tarhouni, J. Development of Water Turbidity Index (WTI) and Seasonal Characteristics of Total Suspended Matter (TSM) Spatial Distribution in Ichkeul Lake, a Shallow Brackish Wetland, Northern-East Tunisia. *Environ. Earth Sci.* **2019**, *78*, 228. [CrossRef]
154. Dogliotti, A.I.; Gossn, J.I.; Vanhellemont, Q.; Ruddick, K.G. Detecting and Quantifying a Massive Invasion of Floating Aquatic Plants in the Río de La Plata Turbid Waters Using High Spatial Resolution Ocean Color Imagery. *Remote Sens.* **2018**, *10*, 1140. [CrossRef]
155. Knaeps, E.; Ruddick, K.G.; Doxaran, D.; Dogliotti, A.I.; Nechad, B.; Raymaekers, D.; Sterckx, S. A SWIR Based Algorithm to Retrieve Total Suspended Matter in Extremely Turbid Waters. *Remote Sens. Environ.* **2015**, *168*, 66–79. [CrossRef]
156. Dewidar, K.; Ezaby, K.E.; Daym, H.A.; Ibrahim, M. Mapping Some Water Quality Parameters by Using Landsat-7 ETM + for Manzala Lagoon, Egypt. In Proceedings of the Environmental Sciences & Technology, Cairo, Egypt, 1–3 April 2008.
157. KC, A.; Chalise, A.; Parajuli, D.; Dhital, N.; Shrestha, S.; Kandel, T. Surface Water Quality Assessment Using Remote Sensing, Gis and Artificial Intelligence. *Technol. J.* **2019**, *1*, 113–122. [CrossRef]
158. Bernier, P.Y. Microwave Remote Sensing of Snowpack Properties: Potential and Limitations. *Nord. Hydrol.* **1987**, *18*, 1–20. [CrossRef]
159. Government of Canada. Microwave Remote Sensing Introduction. Available online: https://www.nrcan.gc.ca/maps-tools-and-publications/satellite-imagery-and-air-photos/tutorial-fundamentals-remote-sensing/microwave-remote-sensing/9371 (accessed on 12 July 2023).
160. Herndon, K.; Meyer, F.; Flores, A.; Cherrington, E.; Kucera, L. What Is Synthetic Aperture Radar? | Earthdata. Available online: https://www.earthdata.nasa.gov/learn/backgrounders/what-is-sar (accessed on 12 July 2023).
161. Zhang, K.; Amineh, R.K.; Dong, Z.; Nadler, D. Microwave Sensing of Water Quality. *IEEE Access* **2019**, *7*, 69481–69493. [CrossRef]
162. Carter, W.D.; Engman, E.T. *Remote Sensing from Satellites*; Elsevier Inc.: Amsterdam, The Netherlands, 1984; ISBN 0080327516.
163. Engman, E.T. Remote Sensing in Hydrology. *Geophys. Monogr. Ser.* **1998**, *108*, 165–177. [CrossRef]
164. Koponen, S.; Pulliainen, J.; Kallio, K.; Hallikainen, M. Lake Water Quality Classification with Airborne Hyperspectral Spectrometer and Simulated MERIS Data. *Remote Sens. Environ.* **2002**, *79*, 51–59. [CrossRef]
165. Doerffer, R.; Schiller, H. The MERIS Case 2 Water Algorithm. *Int. J. Remote Sens.* **2007**, *28*, 517–535. [CrossRef]
166. Myint, S.W.; Walker, N.D. Quantification of Surface Suspended Sediments along a River Dominated Coast with NOAA AVHRR and Sea WiFS Measurements: Louisiana, USA. *Int. J. Remote Sens.* **2002**, *23*, 3229–3249. [CrossRef]
167. Gholizadeh, M.H.; Melesse, A.M.; Reddi, L. Spaceborne and Airborne Sensors in Water Quality Assessment. *Int. J. Remote Sens.* **2016**, *37*, 3143–3180. [CrossRef]
168. Allbed, A.; Kumar, L. Soil Salinity Mapping and Monitoring in Arid and Semi-Arid Regions Using Remote Sensing Technology: A Review. *Adv. Remote Sens.* **2013**, *2*, 373–385. [CrossRef]
169. Fan, C. Spectral Analysis of Water Reflectance for Hyperspectral Remote Sensing of Water Quailty in Estuarine Water. *J. Geosci. Environ. Prot.* **2014**, *2*, 19–27. [CrossRef]
170. Terentev, A.; Dolzhenko, V.; Fedotov, A.; Eremenko, D. Current State of Hyperspectral Remote Sensing for Early Plant Disease Detection: A Review. *Sensors* **2022**, *22*, 757. [CrossRef] [PubMed]
171. Topp, S.N.; Pavelsky, T.M.; Jensen, D.; Simard, M.; Ross, M.R.V. Research Trends in the Use of Remote Sensing for Inland Water Quality Science: Moving towards Multidisciplinary Applications. *Water* **2020**, *12*, 169. [CrossRef]
172. McCarthy, M.J.; Colna, K.E.; El-Mezayen, M.M.; Laureano-Rosario, A.E.; Méndez-Lázaro, P.; Otis, D.B.; Toro-Farmer, G.; Vega-Rodriguez, M.; Muller-Karger, F.E. Satellite Remote Sensing for Coastal Management: A Review of Successful Applications. *Environ. Manag.* **2017**, *60*, 323–339. [CrossRef] [PubMed]
173. European Space Agency. SAR (ERS) Overview. Available online: http://earth.esa.int/eogateway/instruments/sar-ers/description (accessed on 12 July 2023).
174. Li, X.; Ding, J.; Ilyas, N. Machine Learning Method for Quick Identification of Water Quality Index (WQI) Based on Sentinel-2 MSI Data: Ebinur Lake Case Study. *Water Sci. Technol. Water Supply* **2021**, *21*, 1291–1312. [CrossRef]
175. Runge, A.; Grosse, G. Comparing Spectral Characteristics of Landsat-8 and Sentinel-2 Same-Day Data for Arctic-Boreal Regions. *Remote Sens.* **2019**, *11*, 1730. [CrossRef]
176. Meijerink, A.M.J.; Bannert, D.; Batelaan, O.; Lubczynski, M.W.; Pointet, T. *Remote Sensing Applications to Groundwater*; UNESCO: Paris, France, 2007.
177. Wu, M.; Zhang, W.; Wang, X.; Luo, D. Application of MODIS Satellite Data in Monitoring Water Quality Parameters of Chaohu Lake in China. *Environ. Monit. Assess.* **2009**, *148*, 255–264. [CrossRef] [PubMed]
178. National Aeronautics and Space Administration. MODIS. Available online: https://aqua.nasa.gov/modis#:~:text=ThefirstMODISinstrumentwas,onAquainMay2002.&text=SelectedforflightonTerra,%2Ccross-trackscanningradiometer (accessed on 26 June 2023).
179. Sahoo, D.P.; Sahoo, B.; Tiwari, M.K. MODIS-Landsat Fusion-Based Single-Band Algorithms for TSS and Turbidity Estimation in an Urban-Waste-Dominated River Reach. *Water Res.* **2022**, *224*, 119082. [CrossRef]

180. Balasubramanian, S.V.; Pahlevan, N.; Smith, B.; Binding, C.; Schalles, J.; Loisel, H.; Gurlin, D.; Greb, S.; Alikas, K.; Randla, M.; et al. Robust Algorithm for Estimating Total Suspended Solids (TSS) in Inland and Nearshore Coastal Waters. *Remote Sens. Environ.* **2020**, *246*, 111768. [CrossRef]
181. Niroumand-Jadidi, M.; Bovolo, F.; Bresciani, M.; Gege, P.; Giardino, C. Water Quality Retrieval from Landsat-9 (OLI-2) Imagery and Comparison to Sentinel-2. *Remote Sens.* **2022**, *14*, 4596. [CrossRef]
182. Sa'ad, F.N.A.; Tahir, M.S.; Jemily, N.H.B.; Ahmad, A.; Amin, A.R.M. Monitoring Total Suspended Sediment Concentration in Spatiotemporal Domain over Teluk Lipat Utilizing Landsat 8 (OLI). *Appl. Sci.* **2021**, *11*, 7082. [CrossRef]
183. Bhatti, A.M.; Rundquist, D.C.; Nasu, S.; Takagi, M. Assessing the Potential of Remotely Sensed Data for Water Quality Monitoring of Coastal and Inland Waters. *Soc. Soc. Manag. Syst.* **2008**, *5*, 1–7.
184. The European Space Agency. SPOT 6—Earth Online. Available online: https://earth.esa.int/eogateway/missions/spot-6 (accessed on 27 June 2023).
185. Brando, V.E.; Dekker, A.G. Satellite Hyperspectral Remote Sensing for Estimating Estuarine and Coastal Water Quality. *IEEE Trans. Geosci. Remote Sens.* **2003**, *41*, 1378–1387. [CrossRef]
186. Son, S.H.; Kim, Y.H.; Kwon, J., II; Kim, H.C.; Park, K.S. Characterization of Spatial and Temporal Variation of Suspended Sediments in the Yellow and East China Seas Using Satellite Ocean Color Data. *GIScience Remote Sens.* **2014**, *51*, 212–226. [CrossRef]
187. Aguirre-Gomez, R. Detection of Total Suspended Sediments in the North Sea Using AVHRR and Ship Data. *Int. J. Remote Sens.* **2000**, *21*, 1583–1596. [CrossRef]
188. Payra, S.; Sharma, A.; Verma, S. Application of Remote Sensing to Study Forest Fires. In *Atmospheric Remote Sensing*; Elsevier: Amsterdam, The Netherlands, 2023; pp. 239–260. [CrossRef]
189. Maliki, A.A.A.; Chabuk, A.; Sultan, M.A.; Hashim, B.M.; Hussain, H.M.; Al-Ansari, N. Estimation of Total Dissolved Solids in Water Bodies by Spectral Indices Case Study: Shatt Al-Arab River. *Water. Air. Soil Pollut.* **2020**, *231*, 482. [CrossRef]
190. Adjovu, G.E.; Ahmad, S.; Stephen, H. Analysis of Suspended Material in Lake Mead Using Remote Sensing Indices. In Proceedings of the World Environmental and Water Resources Congress 2021, Virtually, 7–11 June 2021. [CrossRef]
191. Johnson, R.W.; Harriss, R.C. Remote Sensing for Water Quality and Biological Measurements in Coastal Waters. *Photogramm. Eng. Remote Sens.* **1980**, *46*, 77–85.
192. Zhang, Y.; Pulliainen, J.; Koponen, S.; Hallikainen, M. Application of an Empirical Neural Network to Surface Water Quality Estimation in the Gulf of Finland Using Combined Optical Data and Microwave Data. *Remote Sens. Environ.* **2002**, *81*, 327–336. [CrossRef]
193. Wilson, W.J.; Yueh, S.H.; Dinardo, S.J.; Chazanoff, S.L.; Kitiyakara, A.; Li, F.K.; Rahmat-Samii, Y. Passive Active L- and S-Band (PALS) Microwave Sensor for Ocean Salinity and Soil Moisture Measurements. *IEEE Trans. Geosci. Remote Sens.* **2001**, *39*, 1039–1048. [CrossRef]
194. Reul, N.; Grodsky, S.A.; Arias, M.; Boutin, J.; Catany, R.; Chapron, B.; D'Amico, F.; Dinnat, E.; Donlon, C.; Fore, A.; et al. Sea Surface Salinity Estimates from Spaceborne L-Band Radiometers: An Overview of the First Decade of Observation (2010–2019). *Remote Sens. Environ.* **2020**, *242*, 111769. [CrossRef]
195. Khan, N.M.; Rastoskuev, V.V.; Sato, Y.; Shiozawa, S. Assessment of Hydrosaline Land Degradation by Using a Simple Approach of Remote Sensing Indicators. *Agric. Water Manag.* **2005**, *77*, 96–109. [CrossRef]
196. Herrault, P.A.; Gandois, L.; Gascoin, S.; Tananaev, N.; Le Dantec, T.; Teisserenc, R. Using High Spatio-Temporal Optical Remote Sensing to Monitor Dissolved Organic Carbon in the Arctic River Yenisei. *Remote Sens.* **2016**, *8*, 803. [CrossRef]
197. Gallagher, L.C. *Dissolved Organic Matter in Coastal and Inland Waters*; University of Victoria: Victoria, BC, Canada, 2004.
198. Montalvo, L.G. *Spectral Analysis of Suspended Material in Coastal Waters: A Comparison between Band Math Equations*; Department of Geology, University of Puerto Rico: Mayaguez, PR, USA, 2010; pp. 1–6.
199. Arisanty, D.; Nur Saputra, A. Remote Sensing Studies of Suspended Sediment Concentration Variation in Barito Delta. *IOP Conf. Ser. Earth Environ. Sci.* **2017**, *98*, 1–6. [CrossRef]
200. Malahlela, O.E. Spatio-Temporal Assessment of Inland Surface Water Quality Using Remote Sensing Data in the Wake of Changing Climate. *IOP Conf. Ser. Earth Environ. Sci.* **2019**, *227*, 062012. [CrossRef]
201. Abbas, A.; Khan, S. *Using Remote Sensing Techniques for Appraisal of Irrigated Soil Salinity*; Modelling and Simulation Society of Australia and New Zealand: Canberra, Australia, 2007; pp. 2632–2638.
202. Veronez, M.R.; Kupssinskü, L.S.; Guimarães, T.T.; Koste, E.C.; Da Silva, J.M.; De Souza, L.V.; Oliverio, W.F.M.; Jardim, R.S.; Koch, I.; De Souza, J.G.; et al. Proposal of a Method to Determine the Correlation between Total Suspended Solids and Dissolved Organic Matter in Water Bodies from Spectral Imaging and Artificial Neural Networks. *Sensors* **2018**, *18*, 159. [CrossRef] [PubMed]
203. Mustafa, M.T.; Hassoon, K.I.; Hussain, H.M.; Abd, M.H. Using Water Indices (NDWI, MNDWI, NDMI, WRI and AWEI) To Detect Physical and Chemical Parameters By Apply Remote Sensing and Gis Techniques. *Int. J. Res.—Granthaalayah* **2017**, *5*, 117–128. [CrossRef]
204. Abdullah, H.S.A.; Mahdi, M.S.M.; Ibrahim, H.M.I. Water Quality Assessment Models for Dokan Lake Using Landsat 8 OLI Satellite Images. *J. Zankoy Sulaimani—Part A* **2017**, *19*, 25–42. [CrossRef]
205. Aral, M.M. Water Quality, Exposure and Health: Purpose and Goals. *Water Qual. Expo. Health* **2009**, *1*, 1–4. [CrossRef]
206. Abdelmalik, K.W. Role of Statistical Remote Sensing for Inland Water Quality Parameters Prediction. *Egypt. J. Remote Sens. Sp. Sci.* **2018**, *21*, 193–200. [CrossRef]

207. United States Geology Survey (USGS). What Are the Band Designations for the Landsat Satellites? Available online: https://www.usgs.gov/faqs/what-are-band-designations-landsat-satellites (accessed on 3 July 2023).
208. Elmahdy, S.I.; Mohamed, M.M. Land Use/Land Cover Change Impact on Groundwater Quantity and Quality: A Case Study of Ajman Emirate, the United Arab Emirates, Using Remote Sensing and GIS. *Arab. J. Geosci.* **2016**, *9*, 722. [CrossRef]
209. Page, B.P.; Olmanson, L.G.; Mishra, D.R. A Harmonized Image Processing Workflow Using Sentinel-2/MSI and Landsat-8/OLI for Mapping Water Clarity in Optically Variable Lake Systems. *Remote Sens. Environ.* **2019**, *231*, 111284. [CrossRef]
210. Pahlevan, N.; Chittimalli, S.K.; Balasubramanian, S.V.; Vellucci, V. Sentinel-2/Landsat-8 Product Consistency and Implications for Monitoring Aquatic Systems. *Remote Sens. Environ.* **2019**, *220*, 19–29. [CrossRef]
211. European Space Agency. Sentinel-2 User Handbook. Available online: https://sentinel.esa.int/documents/247904/685211/sentinel-2_user_handbook (accessed on 3 July 2023).
212. Ferdous, J.; Rahman, M.T.U. Developing an Empirical Model from Landsat Data Series for Monitoring Water Salinity in Coastal Bangladesh. *J. Environ. Manag.* **2020**, *255*, 109861. [CrossRef] [PubMed]
213. Tran1, P.H.; Nguyen, A.K.; Liou, Y.-A.; Hoang, P.P.; Thanh, H.N. Estimation of Salinity Intrusion by Using Landsat 8 OLI Data in The Mekong Delta, Vietnam. *Prog. Earth Planet. Sci.* **2020**, *7*, 1. [CrossRef]
214. Hossain, A.K.M.A.; Chao, X.; Jia, Y. Development of Remote Sensing Based Index for Estimating/Mapping Suspended Sediment Concentration in River and Lake Environments. In Proceedings of the 8th International Symposium on ECOHYDRAULICS, Seoul, Republic of Korea, 12 September 2010; pp. 578–585.
215. Nechad, B.; Ruddick, K.G.; Park, Y. Calibration and Validation of a Generic Multisensor Algorithm for Mapping of Total Suspended Matter in Turbid Waters. *Remote Sens. Environ.* **2010**, *114*, 854–866. [CrossRef]
216. Coskun, H.G.; Tanik, A.; Alganci, U.; Cigizoglu, H.K. Determination of Environmental Quality of a Drinking Water Reservoir by Remote Sensing, GIS and Regression Analysis. *Water. Air. Soil Pollut.* **2008**, *194*, 275–285. [CrossRef]
217. Miller, J.L.; Goodberlet, M. Development and Applications of STARRS: A next Generation Airborne Salinity Imager. *Int. J. Remote Sens.* **2004**, *25*, 1319–1324. [CrossRef]
218. Jin, X.; He, X.; Bai, Y.; Shanmugam, P.; Ying, J.; Gong, F.; Zhu, Q. Assessment and Improvement of Sea Surface Microwave Emission Models for Salinity Retrieval in the East China Sea. *Remote Sens.* **2019**, *11*, 2486. [CrossRef]
219. Vinogradova, N.T.; Ponte, R.M. Small-Scale Variability in Sea Surface Salinity and Implications for Satellite-Derived Measurements. *J. Atmos. Ocean. Technol.* **2013**, *30*, 2689–2694. [CrossRef]
220. Chassignet, E.P.; Hurlburt, H.E.; Metzger, E.J.; Smedstad, O.M.; Cummings, J.A.; Halliwell, G.R.; Bleck, R.; Baraille, R.; Wallcraft, A.J.; Lozano, C.; et al. Global Ocean Prediction with the Hybrid Coordinate Ocean Model (HYCOM). *Oceanography* **2009**, *22*, 64–75. [CrossRef]
221. Kao, H.Y.; Lagerloef, G.S.E.; Lee, T.; Melnichenko, O.; Meissner, T.; Hacker, P. Assessment of Aquarius Sea Surface Salinity. *Remote Sens.* **2018**, *10*, 1341. [CrossRef]
222. D'Sa, E.J.; Zaitzeff, J.B.; Steward, R.G. Monitoring Water Quality in Florida Bay with Remotely Sensed Salinity and in Situ Bio-Optical Observations. *Int. J. Remote Sens.* **2000**, *21*, 811–816. [CrossRef]
223. Ray, R.; Mandal, S.; Dhara, A. Environmental Monitoring of Estuaries: Estimating and Mapping Various Environmental Indicators in Matla Estuarine Complex, Using Landsat TM Digital Data. *Int. J. Geomat. Geosci.* **2013**, *3*, 570–581. [CrossRef]
224. Chao, X.; Jia, Y.; Azad Hossain, A.K.M. Numerical Modeling of Sediment Transport and Its Effect on Algal Biomass Distribution in Lake Pontchartrain Due to Flood Release from Bonnet Carré Spillway. *J. Geosci. Environ. Prot.* **2016**, *4*, 64–79. [CrossRef]
225. Hu, C.; Chen, Z.; Clayton, T.D.; Swarzenski, P.; Brock, J.C.; Muller-Karger, F.E. Assessment of Estuarine Water-Quality Indicators Using MODIS Medium-Resolution Bands: Initial Results from Tampa Bay, FL. *Remote Sens. Environ.* **2004**, *93*, 423–441. [CrossRef]
226. Miller, R.L.; McKee, B.A. Using MODIS Terra 250 m Imagery to Map Concentrations of Total Suspended Matter in Coastal Waters. *Remote Sens. Environ.* **2004**, *93*, 259–266. [CrossRef]
227. Doxaran, D.; Cherukuru, R.C.N.; Lavender, S.J. Use of Reflectance Band Ratios to Estimate Suspended and Dissolved Matter Concentrations in Estuarine Waters. *Int. J. Remote Sens.* **2005**, *26*, 1763–1769. [CrossRef]
228. Hafeez, S.; Wong, M.S.; Ho, H.C.; Nazeer, M.; Nichol, J.; Abbas, S.; Tang, D.; Lee, K.H.; Pun, L. Comparison of Machine Learning Algorithms for Retrieval of Water Quality Indicators in Case-II Waters: A Case Study of Hong Kong. *Remote Sens.* **2019**, *11*, 617. [CrossRef]
229. Sudheer, K.P.; Chaubey, I.; Garg, V. Lake Water Quality Assessment from Landsat Thematic Mapper Data Using Neural Network: An Approach to Optimal Band Combination Selection. *J. Am. Water Resour. Assoc.* **2006**, *42*, 1683–1695. [CrossRef]
230. Song, K.; Li, L.; Li, S.; Tedesco, L.; Hall, B.; Li, L. Hyperspectral Remote Sensing of Total Phosphorus (TP) in Three Central Indiana Water Supply Reservoirs. *Water Air Soil Pollut.* **2012**, *223*, 1481–1502. [CrossRef]
231. AL-Fahdawi, A.A.H.; Rabee, A.M.; Al-Hirmizy, S.M. Water Quality Monitoring of Al-Habbaniyah Lake Using Remote Sensing and in Situ Measurements. *Environ. Monit. Assess.* **2015**, *187*, 367. [CrossRef]
232. Li, J.; Chen, X.; Tian, L.; Huang, J.; Feng, L. Improved Capabilities of the Chinese High-Resolution Remote Sensing Satellite GF-1 for Monitoring Suspended Particulate Matter (SPM) in Inland Waters: Radiometric and Spatial Considerations. *ISPRS J. Photogramm. Remote Sens.* **2015**, *106*, 145–156. [CrossRef]
233. Masocha, M.; Murwira, A.; Magadza, C.H.D.; Hirji, R.; Dube, T. Remote Sensing of Surface Water Quality in Relation to Catchment Condition in Zimbabwe. *Phys. Chem. Earth* **2017**, *100*, 13–18. [CrossRef]

234. Isidro, C.M.; McIntyre, N.; Lechner, A.M.; Callow, I. Quantifying Suspended Solids in Small Rivers Using Satellite Data. *Sci. Total Environ.* **2018**, *634*, 1554–1562. [CrossRef]
235. Deutsch, E.S.; Alameddine, I.; El-Fadel, M. Monitoring Water Quality in a Hypereutrophic Reservoir Using Landsat ETM+ and OLI Sensors: How Transferable Are the Water Quality Algorithms? *Environ. Monit. Assess.* **2018**, *190*, 141. [CrossRef] [PubMed]
236. Saberioon, M.; Brom, J.; Nedbal, V.; Souček, P.; Císarč, P. Chlorophyll-a and Total Suspended Solids Retrieval and Mapping Using Sentinel-2A and Machine Learning for Inland Waters. *Ecol. Indic.* **2020**, *113*, 106236. [CrossRef]
237. Japitana, M.V.; Burce, M.E.C. A Satellite-Based Remote Sensing Technique for Surface Water Quality Estimation. *Eng. Technol. Appl. Sci. Res.* **2019**, *9*, 3965–3970. [CrossRef]
238. Abbas, M.R.; Rasib, A.W.B.; Ahmad, B.B.; Musa, T.A.B.; Abbas, T.R.; Dutsenwai, H.S. Landsat Data to Estimate a Model of Water Quality Parameters in Tigris and Euphrates Rivers—Iraq. *Int. J. Adv. Appl. Sci.* **2019**, *6*, 50–58. [CrossRef]
239. Aljoborey, A.D.A.; Abdulhay, H.S. Estimating Total Dissolved Solids and Total Suspended Solids in Mosul Dam Lake in Situ and Using Remote Sensing Technique. *Period. Eng. Nat. Sci. USA* **2019**, *7*, 1755–1767. [CrossRef]
240. Kumar, V.; Sharma, A.; Bhardwaj, R.; Thukral, A.K. Water Quality of River Beas, India, and Its Correlation with Reflectance Data. *J. Water Chem. Technol.* **2020**, *42*, 134–141. [CrossRef]
241. Ewusi, A.; Ahenkorah, I.; Aikins, D. Modelling of Total Dissolved Solids in Water Supply Systems Using Regression and Supervised Machine Learning Approaches. *Appl. Water Sci.* **2021**, *11*, 13. [CrossRef]
242. Bayati, M.; Danesh-Yazdi, M. Mapping the Spatiotemporal Variability of Salinity in the Hypersaline Lake Urmia Using Sentinel-2 and Landsat-8 Imagery. *J. Hydrol.* **2021**, *595*, 126032. [CrossRef]
243. Ferdous, J.; Ur Rahman, M.T.; Ghosh, S.K. Detection of Total Dissolved Solids from Landsat 8 OLI Image in Coastal Bangladesh. *Int. Conf. Clim. Chang.* **2019**, *3*, 35–44. [CrossRef]
244. Ali Shaikh, T.; Ahmad, S.; Stephen, H. Assessing Spatiotemporal Change in Land Cover and Total Dissolved Solids Concentration Using Remote Sensing Data. In Proceedings of the World Environmental and Water Resources Congress, Virtually, 7–11 June 2021; American Society of Civil Engineers: Reston, VA, USA, 2021; pp. 384–396.
245. Batur, E.; Maktav, D. Assessment of Surface Water Quality by Using Satellite Images Fusion Based on PCA Method in the Lake Gala, Turkey. *IEEE Trans. Geosci. Remote Sens.* **2019**, *57*, 2983–2989. [CrossRef]
246. Ansari, M.; Akhoondzadeh, M. Mapping Water Salinity Using Landsat-8 OLI Satellite Images (Case Study: Karun Basin Located in Iran). *Adv. Space Res.* **2020**, *65*, 1490–1502. [CrossRef]
247. Sun, D.; Su, X.; Qiu, Z.; Wang, S.; Mao, Z.; He, Y. Remote Sensing Estimation of Sea Surface Salinity from GOCI Measurements in the Southern Yellow Sea. *Remote Sens.* **2019**, *11*, 775. [CrossRef]
248. Zhao, J.; Temimi, M.; Ghedira, H. Remotely Sensed Sea Surface Salinity in the Hyper-Saline Arabian Gulf: Application to Landsat 8 OLI Data. *Estuar. Coast. Shelf Sci.* **2017**, *187*, 168–177. [CrossRef]
249. Somvanshi, S.; Kunwar, P.; Singh, N.B.; Shukla, S.P.; Pathak, V. Integrated Remote Sensing and GIS Approach for Water Quality Analysis of Gomti River, Uttar Pradesh. *Int. J. Environ. Sci.* **2012**, *3*, 62–75. [CrossRef]
250. Xu, H.; Xu, G.; Wen, X.; Hu, X.; Wang, Y. Lockdown Effects on Total Suspended Solids Concentrations in the Lower Min River (China) during COVID-19 Using Time-Series Remote Sensing Images. *Int. J. Appl. Earth Obs. Geoinf.* **2021**, *98*, 102301. [CrossRef]
251. Jiang, D.; Matsushita, B.; Pahlevan, N.; Gurlin, D.; Lehmann, M.K.; Fichot, C.G.; Schalles, J.; Loisel, H.; Binding, C.; Zhang, Y.; et al. Remotely Estimating Total Suspended Solids Concentration in Clear to Extremely Turbid Waters Using a Novel Semi-Analytical Method. *Remote Sens. Environ.* **2021**, *258*, 112386. [CrossRef]
252. Di Trapani, A.; Corbari, C.; Mancini, M. Effect of the Three Gorges Dam on Total Suspended Sediments from Modis and Landsat Satellite Data. *Water* **2020**, *12*, 3259. [CrossRef]
253. Chen, J.; Quan, W.; Cui, T.; Song, Q. Estimation of Total Suspended Matter Concentration from MODIS Data Using a Neural Network Model in the China Eastern Coastal Zone. *Estuar. Coast. Shelf Sci.* **2015**, *155*, 104–113. [CrossRef]
254. Kang, W.; Lee, K.; Kim, S. Use of Underwater-Image Color to Determine Suspended-Sediment Concentrations Transported to Coastal Regions. *Appl. Sci.* **2023**, *13*, 7219. [CrossRef]
255. Hamidi, S.A.; Hosseiny, H.; Ekhtari, N.; Khazaei, B. Using MODIS Remote Sensing Data for Mapping the Spatio-Temporal Variability of Water Quality and River Turbid Plume. *J. Coast. Conserv.* **2017**, *21*, 939–950. [CrossRef]
256. Yepez, S.; Laraque, A.; Martinez, J.M.; De Sa, J.; Carrera, J.M.; Castellanos, B.; Gallay, M.; Lopez, J.L. Retrieval of Suspended Sediment Concentrations Using Landsat-8 OLI Satellite Images in the Orinoco River (Venezuela). *Comptes Rendus—Geosci.* **2018**, *350*, 20–30. [CrossRef]
257. Wang, C.; Chen, S.; Li, D.; Wang, D.; Liu, W.; Yang, J. A Landsat-Based Model for Retrieving Total Suspended Solids Concentration of Estuaries and Coasts in China. *Geosci. Model Dev.* **2017**, *10*, 4347–4365. [CrossRef]
258. Chen, J.; Cui, T.; Qiu, Z.; Lin, C. A Three-Band Semi-Analytical Model for Deriving Total Suspended Sediment Concentration from HJ-1A/CCD Data in Turbid Coastal Waters. *ISPRS J. Photogramm. Remote Sens.* **2014**, *93*, 1–13. [CrossRef]
259. Sharaf El Din, E.; Zhang, Y.; Suliman, A. Mapping Concentrations of Surface Water Quality Parameters Using a Novel Remote Sensing and Artificial Intelligence Framework. *Int. J. Remote Sens.* **2017**, *38*, 1023–1042. [CrossRef]
260. Braga, F.; Giardino, C.; Bassani, C.; Matta, E.; Candiani, G.; Strömbeck, N.; Adamo, M.; Bresciani, M. Assessing Water Quality in the Northern Adriatic Sea from Hicotm Data. *Remote Sens. Lett.* **2013**, *4*, 1028–1037. [CrossRef]
261. Normand, A.E. *Landsat 9 and the Future of the Sustainable Land Imaging Program*; Congressional Research Service: Washington, DC, USA, 2020; pp. 1–31.

262. Olmanson, L.G.; Brezonik, P.L.; Bauer, M.E. Evaluation of Medium to Low Resolution Satellite Imagery for Regional Lake Water Quality Assessments. *Water Resour. Res.* **2011**, *47*, 1–14. [CrossRef]
263. Garcia, R.A.; Lee, Z.; Hochberg, E.J. Hyperspectral Shallow-Water Remote Sensing with an Enhanced Benthic Classifier. *Remote Sens.* **2018**, *10*, 147. [CrossRef]
264. Lyzenga, D.R. Remote Sensing of Bottom Reflectance and Water Attenuation Parameters in Shallow Water Using Aircraft and Landsat Data. *Int. J. Remote Sens.* **1981**, *2*, 71–82. [CrossRef]
265. Rahman, M.T. Applications of Active Remote Sensing Technologies for Natural Disaster Damage Assessments. In *Remote Sensing Techniques and GIS Applications in Earth and Environmental Studies*; IGI Global: Hershey, PA, USA, 2017; pp. 212–227. ISBN 978-1-5225-1814-3.
266. Chang, J.; Clay, E.D. Chapter 22: Matching Remote Sensing to Problems. In *iGrow Corn: Best Management Practices*; South Dakota State University: Brookings, SD, USA, 2016.
267. Song, K.; Li, L.; Wang, Z.; Liu, D.; Zhang, B.; Xu, J.; Du, J.; Li, L.; Li, S.; Wang, Y. Retrieval of Total Suspended Matter (TSM) and Chlorophyll-a (Chl-a) Concentration from Remote-Sensing Data for Drinking Water Resources. *Environ. Monit. Assess.* **2011**, *184*, 1449–1470. [CrossRef] [PubMed]
268. Abdelal, Q.; Assaf, M.N.; Al-Rawabdeh, A.; Arabasi, S.; Rawashdeh, N.A. Assessment of Sentinel-2 and Landsat-8 OLI for Small-Scale Inland Water Quality Modeling and Monitoring Based on Handheld Hyperspectral Ground Truthing. *J. Sens.* **2022**, *2022*, 4643924. [CrossRef]
269. Dunn, A.M.; Hofmann, O.S.; Waters, B.; Witchel, E. Cloaking Malware with the Trusted Platform Module. In Proceedings of the 20th USENIX Security Symposium (USENIX Security 11), San Francisco, CA, USA, 10–12 August 2011; pp. 395–410.
270. Bui, Q.T.; Jamet, C.; Vantrepotte, V.; Mériaux, X.; Cauvin, A.; Mograne, M.A. Evaluation of Sentinel-2/MSI Atmospheric Correction Algorithms over Two Contrasted French Coastal Waters. *Remote Sens.* **2022**, *14*, 1099. [CrossRef]
271. Adjovu, G.E. Evaluating the Performance of A GIS-Based Tool for Delineating Swales Along Two Highways in Tennessee. Master's Thesis, Tennessee Technological University, Cookeville, TN, USA, 2020.
272. Moriasi, D.N.; Arnold, J.G.; Van Liew, M.W.; Bingner, R.L.; Harmel, R.D.; Veith, T.L. Model Evaluation Guidelines for Systematic Quantification of Accuracy in Watershed Simulations. *Trans. ASABE* **2007**, *50*, 885–900. [CrossRef]
273. da Silva, M.G.; de Aguiar Netto, A.d.O.; de Jesus Neves, R.J.; do Vasco, A.N.; Almeida, C.; Faccioli, G.G. Sensitivity Analysis and Calibration of Hydrological Modeling of the Watershed Northeast Brazil. *J. Environ. Prot.* **2015**, *6*, 837–850. [CrossRef]
274. Adjovu, G.E.; Gamble, R. Development of HEC-HMS Model for the Cane Creek Watershed. In Proceedings of the 28th Tennessee Water Resources Symposium Tennessee Section of the American Water Resources Association, Montgomery Bell State Park, Burns, TN, USA, 10–12 April 2019; Tennessee Section of the American Water Resources Association: Nashville, TN, USA, 2019; pp. 1C-2–1C-6. Available online: https://img1.wsimg.com/blobby/go/12ed7af3-57dc-468c-af58-da8360f35f16/downloads/Proceedings2019.pdf?ver=1618503482462 (accessed on 12 July 2023).
275. Li, Y.; Li, X.; Xu, C.; Tang, X. Dissolved Oxygen Prediction Model for the Yangtze River Estuary Basin Using IPSO-LSSVM. *Water* **2023**, *15*, 2206. [CrossRef]
276. Wang, X.; Zhang, F.; Ding, J. Evaluation of Water Quality Based on a Machine Learning Algorithm and Water Quality Index for the Ebinur Lake Watershed, China. *Sci. Rep.* **2017**, *7*, 12858. [CrossRef]
277. Dias, R.L.S.; da Silva, D.D.; Fernandes-Filho, E.I.; do Amaral, C.H.; dos Santos, E.P.; Marques, J.F.; Veloso, G.V. Machine Learning Models Applied to TSS Estimation in a Reservoir Using Multispectral Sensor Onboard to RPA. *Ecol. Inform.* **2021**, *65*, 101414. [CrossRef]
278. Pahlevan, N.; Sarkar, S.; Franz, B.A.; Balasubramanian, S.V.; He, J. Sentinel-2 MultiSpectral Instrument (MSI) Data Processing for Aquatic Science Applications: Demonstrations and Validations. *Remote Sens. Environ.* **2017**, *201*, 47–56. [CrossRef]